

# An evaluation of empirical and statistically based smoke plume injection height parametrisations used within air quality models

Joseph L. Wilkins<sup>id</sup> <sup>A,B,C,G</sup>, George Pouliot<sup>A</sup>, Thomas Pierce<sup>A</sup>, Amber Soja<sup>D,E</sup>,  
Hyundeok Choi<sup>D,E</sup>, Emily Gargulinski<sup>D</sup>, Robert Gilliam<sup>A</sup>, Jeffrey Vukovich<sup>F</sup>,  
and Matthew S. Landis<sup>A</sup>

<sup>A</sup>Office of Research and Development, US Environmental Protection Agency,  
Research Triangle Park, NC 27709, USA.

<sup>B</sup>School of Environmental and Forest Sciences, University of Washington, Seattle,  
WA 98195, USA.

<sup>C</sup>Interdisciplinary Studies Department, Howard University, Washington, DC 20059, USA.

<sup>D</sup>National Institute of Aerospace, Hampton, VA 23666, USA.

<sup>E</sup>NASA Langley Research Center, Hampton, VA 23666, USA.

<sup>F</sup>Office of Air and Radiation, US Environmental Protection Agency, Research Triangle Park,  
NC 27709, USA.

<sup>G</sup>Corresponding author. Email: [joseph.wilkins@howard.edu](mailto:joseph.wilkins@howard.edu)

**Abstract.** Air quality models are used to assess the impact of smoke from wildland fires, both prescribed and natural, on ambient air quality and human health. However, the accuracy of these models is limited by uncertainties in the parametrisation of smoke plume injection height (PIH) and its vertical distribution. We compared PIH estimates from the plume rise method (Briggs) in the Community Multiscale Air Quality (CMAQ) modelling system with observations from the 2013 California Rim Fire and 2017 prescribed burns in Kansas. We also examined PIHs estimated using alternative plume rise algorithms, model grid resolutions and temporal burn profiles. For the Rim Fire, the Briggs method performed as well or better than the alternatives evaluated (mean bias of less than  $\pm 5$ –20% and root mean square error lower than 1000 m compared with the alternatives). PIH estimates for the Kansas prescribed burns improved when the burn window was reduced from the standard default of 12 h to 3 h. This analysis suggests that meteorological inputs, temporal allocation and heat release are the primary drivers for accurately modelling PIH.

**Keywords:** air quality model, CALIOP, ceilometer, MicroPulse scanning lidar, plume rise, prescribed burns, remote sensing, wildfire.

Received 2 September 2020, accepted 9 March 2021, published online 31 January 2022

## Introduction

Worldwide, wildland fires (prescribed and natural) emit large quantities of harmful gas- and particulate-phase pollutants into the atmosphere (Andreae and Merlet 2001; Van der Werf *et al.* 2010). Globally, fire-related air pollutants are estimated to cause up to 330 000 fire-attributable deaths year<sup>-1</sup> (Johnston *et al.* 2012; Lelieveld *et al.* 2015). Across the contiguous United States (USA), the economic cost of wildland fire on human health has been estimated to be ~US\$100 billion and cause ~8500 premature deaths year<sup>-1</sup> (e.g. Rappold *et al.* 2017; Fann *et al.* 2018). To minimise economic losses and impacts on human health related to smoke inhalation and smoke forecast, additional assessments of wildland fire emissions are necessary, because modelled emission estimates and meteorological dispersion contain errors and bias due to data limitations (Goodrick *et al.* 2013; Wilkins *et al.* 2018; Liu *et al.* 2019).

Liu *et al.* (2019) listed knowledge gaps and suggested areas needing wildland fire modelling research. An overarching theme was the vertical distribution of a smoke plume, known as the plume rise parametrisation. Plume rise is controlled by fire and meteorology, which include the energy released by the fire, the size of the combustion zone, fuel composition and ambient atmospheric conditions (Labonne *et al.* 2007; Achtemeier *et al.* 2011; Paugam *et al.* 2016; Walter *et al.* 2016). The height of the plume is commonly referred to as smoke plume injection height (PIH) (e.g. Paugam *et al.* 2016). Inaccurate representation of PIH can seriously compromise air quality model performance (e.g. Achtemeier *et al.* 2011; Mallia *et al.* 2018; Wilkins *et al.* 2018; Liu *et al.* 2019).

Our understanding of wildland smoke behaviour and plume evolution has vastly improved with the use of satellite data (Colarco *et al.* 2004; Al-Saadi *et al.* 2008; Soja *et al.* 2009,

2012; Ichoku *et al.* 2012; Val Martin *et al.* 2018; Sokolik *et al.* 2019), ground-based lidar and Doppler radar (Charland and Clements 2013; Clements and Oliphant 2014; Clements *et al.* 2006, 2007, 2016, 2018; McCarthy *et al.* 2018). Remote sensing data have improved the ability to evaluate plume rise models but there are still inherent limitations, such as with satellite overpass times – some occur late morning before the plume has had a chance to fully develop (Giglio *et al.* 2010). These remote sensing analyses suggest that the plume rise parametrisation problem in models is often linked to the interaction between the smoke plume and the capping inversion at the top of the planetary boundary layer (PBL) (Val Martin *et al.* 2018; Wilkins *et al.* 2020). The likelihood for a smoke plume to penetrate the PBL top varies by fire size, fuel loading and atmospheric conditions and can range from a negligible fraction to full penetration (Kahn *et al.* 2008; Val Martin *et al.* 2010; Tosca *et al.* 2011). It is imperative to model the PBL and stable layer (STL) height correctly, because both the PBL and STL can often act as capping atmospheric layers constraining PIH. For smoke to escape the PBL or STL, the heat from a fire must generate sufficient buoyancy to penetrate these layers. Furthermore, the ability of a smoke plume to penetrate the PBL or STL can be highly dependent on the current atmospheric conditions under which a plume is generated, because they can strongly cap or assist in upward motion of air. Whether a plume remains within or penetrates the PBL or STL strongly influences pollution exposure, duration, transport and chemical residence times (e.g. Westphal and Toon 1991; Wotawa and Trainer 2000; Hyer *et al.* 2007; Wilkins *et al.* 2020).

A widely used plume rise approach in deterministic air quality models (AQMs) is Briggs (1975), but its accuracy and performance have been questioned. It has been reported that the Briggs approach both underestimates plume rise for small fires and overestimates plume rise for large fires (Wilkins *et al.* 2018). Gordon *et al.* (2018) reported a 50% underestimate in stack heights. Other plume height parameterisations exist (e.g. Freitas *et al.* 2007; Rio *et al.* 2010; Sofiev *et al.* 2012); however, implementing these more complex schemes has not always improved model performance (e.g. Freitas *et al.* 2006; Kahn *et al.* 2007; Leung *et al.* 2007; Val Martin *et al.* 2012; Paugam *et al.* 2016). It can be difficult to determine the exact reason for the model uncertainty as it could be related to the plume rise algorithm or the inputs driving the plume rise, i.e. heat flux. Some of these discrepancies are likely related to historic model design, previous state of knowledge and input limitations. Historically, regional and global AQMs did not account for smoke from small fires (<500 ha) that penetrated the PBL (Mims *et al.* 2010; Zhou *et al.* 2018; Baker *et al.* 2019), latent heat releases often seen in fire-generated smoke-infused pyrocumulonimbus thunderstorms (Peterson *et al.* 2015, 2018), or fires that generated multiple cores and were detrained in vertically distinct layers of the atmosphere (Kahn *et al.* 2007; Achtemeier *et al.* 2011; Liu *et al.* 2013; Val Martin *et al.* 2010).

The present study implemented empirical and statistically based plume rise algorithms in an AQM for two conditions: a large wildfire (>6000 ha day<sup>-1</sup>) and a series of small prescribed fires (<500 ha day<sup>-1</sup>). Specific plume rise parameterisations were

chosen by their computational cost to implement in an AQM, ease of implementation and availability of variables. A quantitative assessment of plume rise was then conducted and compared with satellite- and ground-based observation data. The goal of this study was to seek improvement of wildland smoke plume injection heights in the US Environmental Protection Agency (EPA)'s Community Multiscale Air Quality (CMAQ) modelling system.

## Methods and materials

### *Burn sites*

Observational data were obtained from the California Rim Fire in August 2013, representative of a large wildfire (Fig. 1) and the Konza Prairie Biological Station prescribed burn experiment in the Flint Hills, Kansas, in March 2017, representative of a series of small grassland burns (Fig. 2). Table 1 summarises the field-specific information for each of these burns.

#### *Burns 1 and 2: Rim Fire sites*

The Rim Fire was an intense wildfire, burning 104 131 ha, that had an active flaming stage from late August to early September 2013 in the central Sierra Nevada Mountains, California. The Rim Fire contained a few major spread events (periods of rapid growth in burned area) generating plumes that reached well above the PBL as determined by satellite retrievals and aircraft imagery (Peterson *et al.* 2015). The first spread event (Burn 1), between 21 and 23 August 2013, burned 36 206 ha (~35% of the total) and the second spread event (Burn 2), between 25 and 26 August 2013, burned 12 067 ha (~12% of the total). We analysed the first spread event (12 068 ha day<sup>-1</sup>) and the day before the second spread event (6033 ha day<sup>-1</sup>). The ecosystem fuels were mixed forest dominated by a coniferous overstorey and shrubs. Fuel loading was estimated at 1-km resolution using the United States Forest Service Fuel Characteristic Classification System database (McKenzie *et al.* 2007; Ottmar *et al.* 2007; Larkin *et al.* 2009).

#### *Burns 3, 4 and 5: Konza Prairie sites*

During the Konza Prairie prescribed burn, 13 total field units were burned (<4 to 205 ha); however, owing to the size of those individual units, only six fields were chosen for this analysis (threshold >30 ha day<sup>-1</sup>). Four of those six fields were combined into one fire for modelling purposes because they were close in proximity, duration and burn start times. Each of the resulting three Konza Prairie burns (Burns 3, 4 and 5) occurred from late morning to early afternoon on 16 (Burns 3, 4) or 20 March 2017 (Burn 5). The fuel loading was composed of 95% big bluestem grass, switchgrass and Indian grass. The fields were irregularly shaped and followed natural terrain features with roads used as fire breaks (Whitehill *et al.* 2019).

### *Remote sensing of plume height*

Cloud-Aerosol Lidar with Orthogonal Polarisation (CALIOP) is an instrument on the Cloud-Aerosol Lidar and Infrared Pathfinder Satellite Observations (CALIPSO) satellite (Omar *et al.* 2009; Winker *et al.* 2009; <http://www-calipso.larc.nasa.gov/>). CALIOP provides high vertical resolution (30–60 m) 532 nm and 1064 nm (km<sup>-1</sup> sr<sup>-1</sup>) attenuated backscatter data, which can detect both thick and optically thin smoke layers in the atmosphere.

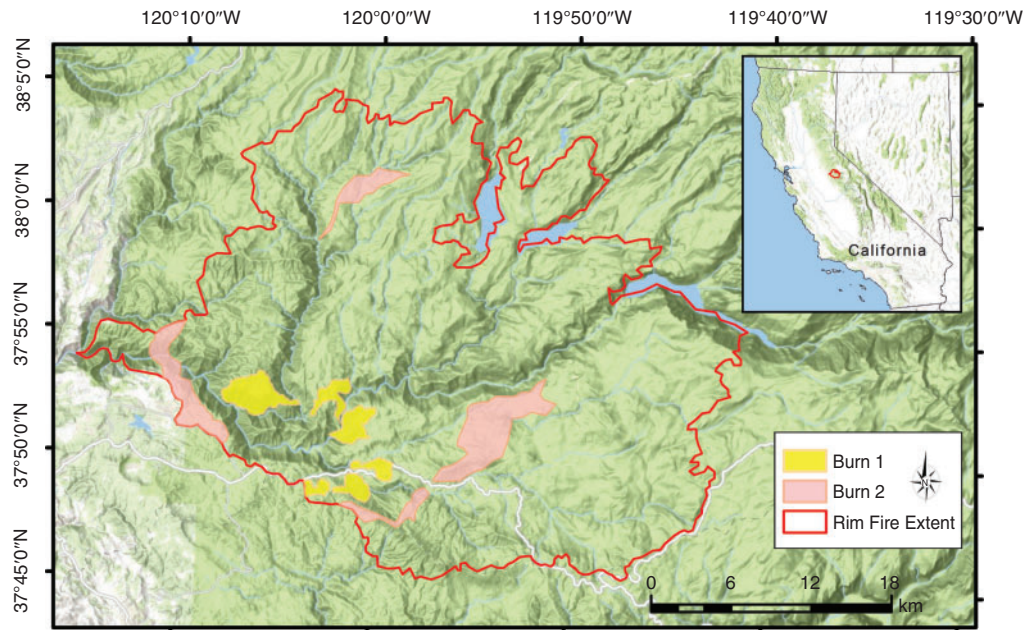


**Fig. 1.** Burned areas from the 2013 California Rim Fire: Burn 1 (21 August, yellow shading), Burn 2 (24 August, pink shading), and the full burned area perimeter (red line).

Standard products include a Vertical Feature Mask, which distinguishes clean air, clouds, stratosphere, surface, subsurface and aerosols, and an Aerosol Subtype product (Fig. 3; additional tracks are shown in Fig. S1, Supplementary material).

#### *Burns 1 and 2: Rim Fire satellite-based PIH*

For the Rim Fire, a satellite-based PIH product was produced by extracting the smoke-filled aerosol parcels from the CALIOP data. Figs 3 and 4 highlight the vertical and the horizontal transport of Rim Fire smoke across several states, where the smoke transected the CALIPSO track. In this case, the smoke extended from  $\sim 5$  km to the surface (Fig. 3). The CALIOP-based plume-detrainment height data used in this work were produced by:

1. overlaying CALIPSO tracks on the NOAA Hazard Mapping System (HMS) smoke product to ensure that the aerosols were smoke (Fig. 4; see Figs S1 and S2 in the Supplementary material for additional CALIPSO tracks);
2. extracting CALIOP aerosol data, which were used to initialise the Langley Trajectory Model (LaTM) (Pierce *et al.* 2003, 2009);
3. the smoke-laden aerosols were then transported backwards in three-dimensional space and time (15-min time steps) until they horizontally coincided with a fire within 20 km (Fig. 5). Fires were determined using daily Moderate Resolution Imaging Spectroradiometer (MODIS) active-fire detection data (Figs 3 and 4; Giglio *et al.* 2003; Soja *et al.* 2012; Thomas *et al.* 2017; Baker *et al.* 2018).

NASA's Modern-Era Retrospective Analysis for Research and Applications, Version 2 (MERRA-2) meteorological data were used to drive LaTM simulations (Gelaro *et al.* 2017). For

details, see Supplementary material S1, CALIOP-derived retrievals.

#### *Burns 3, 4 and 5: Konza Prairie lidar-based PIH*

For the prescribed burns at Konza Prairie, we used a ground-based scanning customised miniaturised version of the Hexagon Micro Pulse Lidar (Spinhirne 1993; Spinhirne *et al.* 1995), hereafter referred to as Mini Micro Pulse Lidar (MiniMPL), following the procedures described by Kovalev *et al.* (2005) and Charland and Clements (2013). The MiniMPL used a combination of plan position indicator (PPI) and range height indicator (RHI) scans to provide near-range atmospheric lidar retrievals of plume tops (Welton and Campbell 2002). For the three Konza Prairie burns (Burns 3, 4, 5), Fig. 6 shows the raw MiniMPL retrievals for Burns 3 and 4 that were converted into PIH (Fig. 7; see Fig. S5 in the Supplementary material for Burn 5 results).

To estimate the PBL height during each of the three Konza Prairie burns, two Vaisala Model CL-51 ceilometers (Münkel *et al.* 2007; McKendry *et al.* 2009, 2010) were also deployed (e.g. Tsaknakis *et al.* 2011; Liu *et al.* 2013; Clements and Oliphant 2014). Operational details for the CL-51 and MiniMPL are summarised in Supplementary material S2 (Operational details for the CL-51 and MiniMPL) and Table S1.

#### *Planetary boundary layer (PBL) plume penetration evaluation*

Prior to evaluating alternative plume rise algorithms against the Briggs method, each model formulation was compared with independently measured or derived PBL heights. For the Rim Fire, we used the MERRA-2 PBL, and for the Konza Prairie prescribed fire, we took the PBL height measurements from the ceilometer and lidar data that were on site (Table 1). We then compared

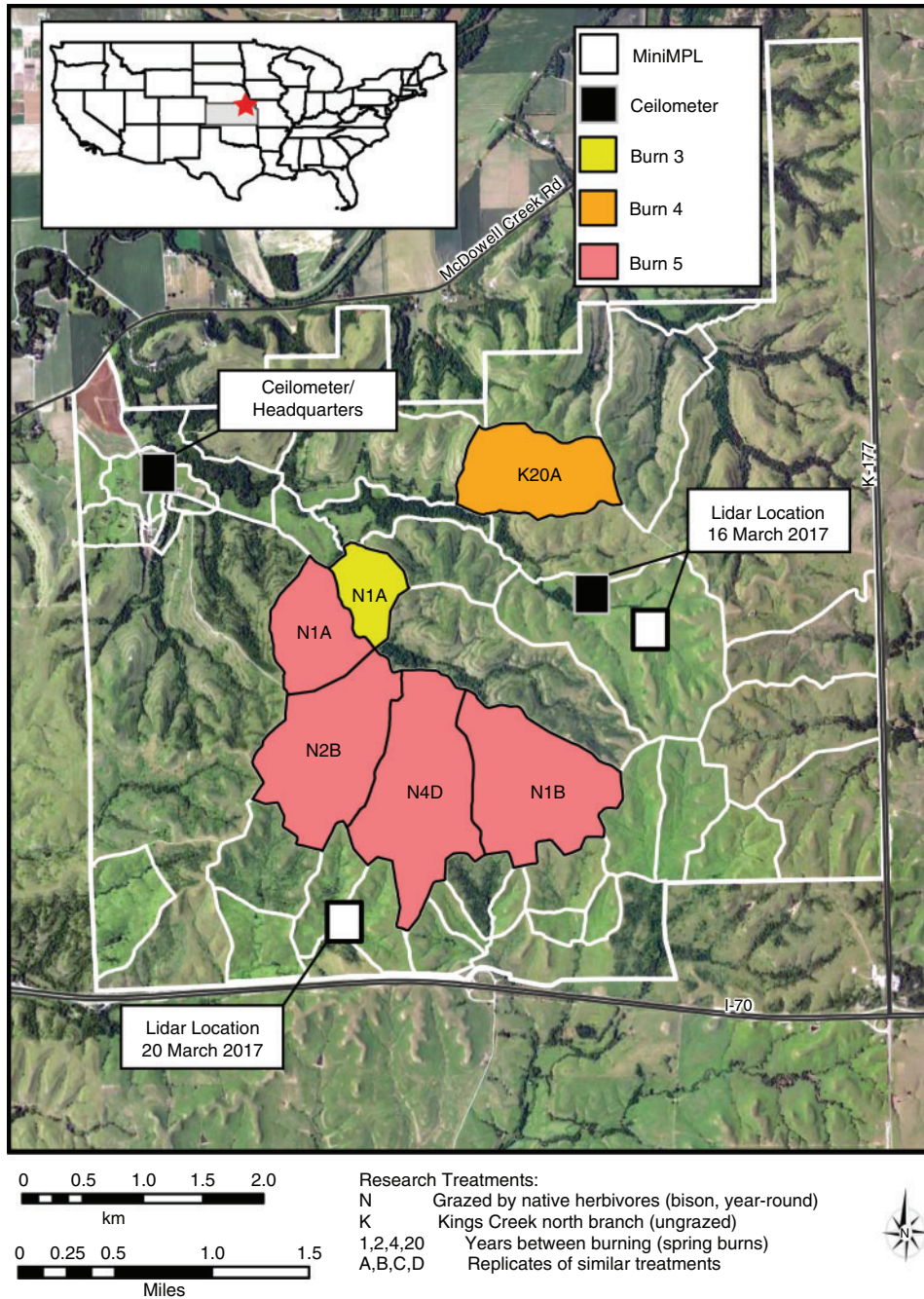


**Fig. 2.** Burned areas from the March 2017 prescribed fire experiment in Konza Prairie, Kansas. Burn units 3, 4 and 5 are shaded yellow, orange and pink, respectively. Also shown are the locations of ground-based Hexagon Miniaturised Micro Pulse Lidar (MiniMPL) (open white squares) and two Vaisala Model CL-51 ceilometers at the Konza Prairie Biological Station (open black squares). For Burns 3 and 4 (16 Mar 17), the MiniMPL and an additional CL-51 to the one placed at Headquarters was deployed. For all other days, only the CL-51 at Headquarters was used.

independent and modelled PBLs to determine model error and bias (Section S3, Planetary boundary layer (PBL) analysis).

*Model parametrisations, sensitivities and comparisons*

To better understand model estimated predictions of PIH, we employed the US EPA’s CMAQ system ([www.epa.gov/cmaq](http://www.epa.gov/cmaq))

with the standard option for plume rise, which uses the Sparse Matrix Operational Kernel for Emissions (SMOKE) as the emissions processing system (Pouliot *et al.* 2005). The CMAQ standard plume rise algorithm is detailed in sections S4 (Smoke model details) and S5 (Weather and Research Forecasting (WRF) model (WRF 12 km and 4 km)).

**Table 1.** Summary of burn information for the California Rim Fire (Burns 1, 2), which burned in August 2013 (from Peterson *et al.* 2015), and the Konza Prairie Biological Station prescribed burn experiment (Burns 3, 4, 5), which burned in the Flint Hills, Kansas, in March 2017 (from Whitehill *et al.* 2019)

Event	Burn	Date	Burn unit	Burn unit size (ha)	Burn time (h)	Fuel loading (kg ha <sup>-1</sup> )	Obs. max. PBL height (m)	Obs. max. Plume top (m)	Plume top above PBL	Obs. method
Rim Fire	1	21 Aug 2013	Spread event 1	6562	12	13 786	2168	6795	✓	CALIOP
Rim Fire	2	24 Aug 2013	Spread event 2	49748	12	13 786	1878	5588	✓	CALIOP
Konza	3	16 Mar 2017	N1A_top	34	1.9	5290	972	600		MiniMPL
Konza	4	16 Mar 2017	K20A	83	1.6	6232	1272	1100		MiniMPL
Konza	5 <sup>A</sup>	20 Mar 2017	N2B, N4D, N1B, N1A_bottom	436	3.6	5649	747	4100	✓	MiniMPL

<sup>A</sup>Burn 5 is a combined four-unit burn, where fields burned both concurrently and side by side. Plume top above the planetary boundary layer (PBL) refers to cases where at least a portion of the plume was observed above the PBL. The Konza PBL data were measured using a ground-based Hexagon Miniaturised Micro Pulse Lidar (MiniMPL) and two Vaisala Model CL-51 ceilometers. For the Rim Fire, the PBL was defined using MERRA-2 meteorological data, and plume tops were derived using CALIOP.

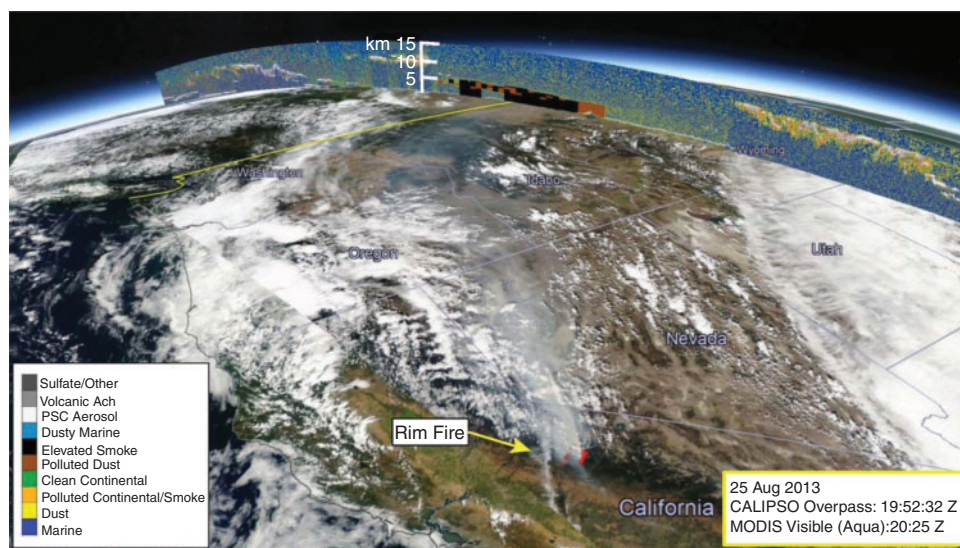


**Fig. 3.** CALIPSO track overlaid on a MODIS Visible image, showing both the vertical and horizontal extent of smoke and clouds. MODIS Terra and Aqua fire detection data (red dots) highlight the Rim Fire burning in California on 25 August 2013. The visible smoke was transported across California, Nevada, Oregon and Idaho before intersecting with the CALIPSO track over Montana and Canada. The CALIOP smoke-aerosol vertical-profile data (black and brown) extend from the surface to ~5 km. The vertical extent and height of the clouds are evident to the south and north of the CALIOP swath, and the horizontal extent of the clouds is evident in the visible MODIS image. CALIOP data provide the vertical properties that inform the horizontal view to provide a complete representation of aerosol transport and the atmosphere.

*Model plume rise parameterisations*

For the Rim Fire, the model was initialised using fire activity data (Sullivan *et al.* 2008) extracted from the BlueSky Framework using SMARTFIRE2 (Raffuse *et al.* 2009, 2012). For the Konza Prairie burns, we used field-specific information provided by Konza Prairie’s Biological Station research staff (Table 1). Parametrisation details for each plume rise method are listed in Table 2 (plume rise model parameterisation), Table 3 (algorithm configurations) and Table S3 (model equations). Specific plume rise parameterisations were chosen by their computational cost to implement in an AQM, ease of implementation and availability of parametrisation variables calculated by CMAQ. A major criticism of the standard

CMAQ-Briggs PIH calculated on a 12-km grid (hereafter BASE12) is that it is based on experimental data from non-fire plumes (i.e. stack point sources). Another critique is that the buoyancy flux calculation may be inappropriate for large fires (Sofiev *et al.* 2012; Zhou *et al.* 2018). To assess these criticisms, we evaluated the CMAQ BASE12 model sensitivity to alternative PIH algorithms, model grid spacing and temporal profiles.

*Model plume rise sensitivities*

To evaluate the BASE12 PIH algorithm sensitivity, we tested two models (Table 2, Table S3). The first model was an empirical energy balance parameterisation (like convective cloud formulations) designed for fires (Sofiev *et al.* 2012), which is implemented at 12- and 4-km grids (hereafter

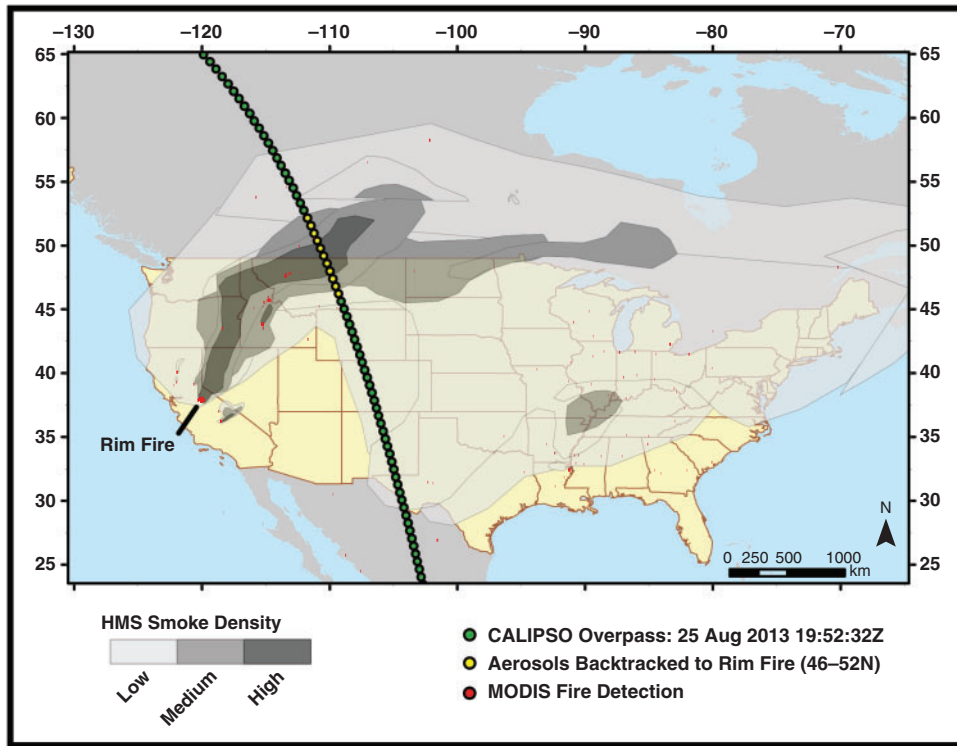


**Fig. 4.** CALIPSO track overpass path on 25 August 2013 (green dots: see Fig. 3) overlaid on a Hazard Mapping System Fire and Smoke (HMS) product with MODIS Terra and Aqua fire detection data (red dots). Map shows the site of the 2013 California Rim Fire. The aerosols backtracked to the Rim Fire were transported across California, Nevada, Oregon and Idaho before intersecting with the CALIPSO track over Montana and Canada (yellow dots).

SOFIEV12KMHR and SOFIEV4KMHR). Sofiev is designed to use Fire Radiative Power (FRP); when available, we used the satellite-based measurements, and when not available, it was derived ( $FRP_{calc} = \text{heat flux} \times 0.1 \times \text{area burned}$ ) using the model heat flux and area burned, assuming that radiative energy was 10% of the total fire heat energy (Wooster *et al.* 2005; Val Martin *et al.* 2012). The alternative model was underpinned by a physical rationale based on fire smoke's general tendency to pool under stable layers (Kahn *et al.* 2007; Val Martin *et al.* 2010). This formulation assumes that a smoke plume will reach the PBL and not rise above that layer. The PBL is not a static parameter; therefore, we added 500 m to the PBL maximum value in the model for each hour simulated. This better represented the maximum PIH potential just reaching above the PBL, based on the hourly time-averaged thickness of the model layer used (hereafter PBL50012KM). See section S6 (Sofiev algorithm explanation) and Table S3 (energy balance equations).

#### Model plume rise comparisons

To evaluate the BASE12 spatial profile sensitivity, a grid spacing of 12 km was compared with the Briggs algorithm at 4 km (hereafter BRIGGS4KMHR); the only difference was the meteorological inputs used at those respective grid resolutions. To evaluate the BASE12 temporal profile sensitivity, as suggested by Zhou *et al.* (2018), we adjusted the temporal profiles from the national-scale modelling standard 12-h profile (0600–1800 Local Standard Time) to a 3- or 4-h profile (from fire start time) on the 12-km grid (hereafter BRIGGS12KMHR).

## Results

### Observations

#### Burn site meteorological conditions and fuels

Table 1 summarises plume rise information for both the 2013 Rim wildfire and 2017 Konza Prairie prescribed fire. Burns 1 and 2 of the Rim Fire (Fig. 1) occurred on 21 and 24 August 2013, respectively, during drought conditions of warm temperatures with low relative humidity ( $RH < 10\%$ ). These conditions caused the fires to spread quickly in winds of  $3\text{--}10\text{ m s}^{-1}$  (Peterson *et al.* 2015). The burned area was greater for Burn 2, but the daily fire spread rate for Burn 1 ( $503\text{ ha h}^{-1}$ ) was double that of Burn 2 ( $251\text{ ha h}^{-1}$ ). At Konza Prairie (Fig. 2), Burns 3 and 4 were conducted on 16 March, and Burn 5 occurred in mid-morning on 20 March (1600 Coordinated Universal Time (UTC)) through early afternoon (2200 UTC). Burns were conducted under the influence of an upper-level trough in a post-frontal air mass and a boundary layer range of 1–2 km by mid-afternoon (2100 UTC). Surface conditions contained a weakening high-pressure system (15 March: 1036.0 hPa; 20 March: 1010.5 hPa), southerly winds ( $2\text{--}5\text{ m s}^{-1}$ ) and moderate  $RH (>20\%)$ . The large-scale patterns of wind, temperature and pressure affecting eastern Kansas during each burn were consistent except for temperature and cloud cover. During the burns, the temperature ranged from  $-4^\circ$  to  $33^\circ\text{C}$ , with low  $RH$  of  $<15\%$ , and light wind speeds of  $<5.5\text{ m s}^{-1}$  (Whitehill *et al.* 2019). The vegetation composition was consistent among burns, with a fuel loading range of  $530\text{--}630\text{ g m}^{-2}$  and an average burn rate of  $32\text{ ha h}^{-1}$ . Details on the meteorological conditions

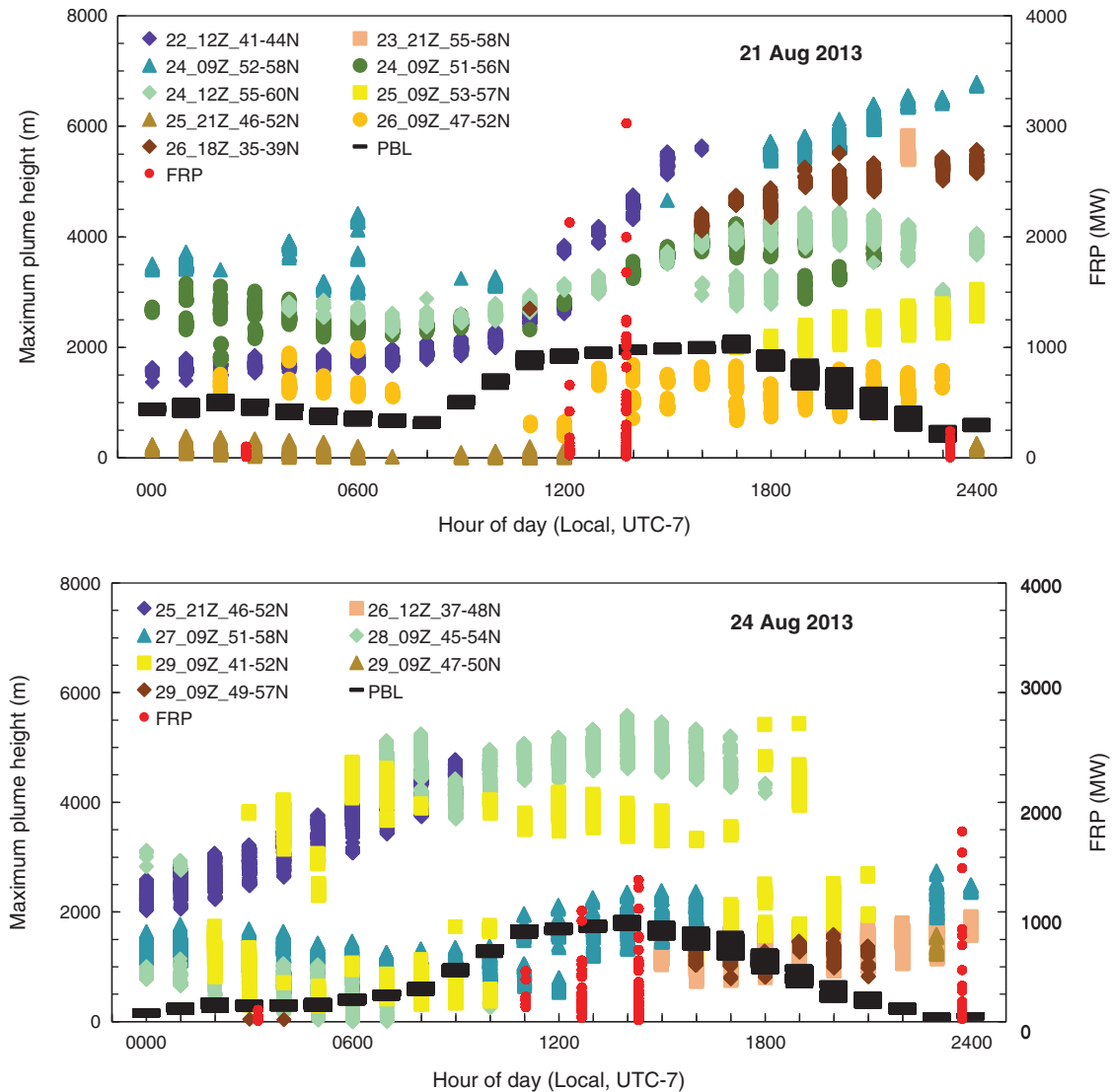


**Fig. 5.** 2013 California Rim Fire. Maximum vertical allocation of smoke-plume tops of Burn 1 (21 August) and Burn 2 (24 August), plotted with the planetary boundary layer (PBL) and fire radiative power (FRP). Smoke plume detrainment was derived using Cloud-Aerosol Lidar with Orthogonal Polarisation (CALIOP) data. Each colour represents a distinct CALIPSO overpass. For example, the 21 August smoke plume was captured by nine distinct CALIOP overpasses, and the 24 August smoke plume was captured by seven CALIOP overpasses. Each CALIOP overpass is named by the date of smoke/CALIOP data coincident, model initialised GMT (Greenwich mean time) time, and the location of the smoke plume in the CALIOP overpass. For example, the smoke represented in purple-blue from 21 August coincided with a CALIOP overpass on 22 August at 41–44°N latitude; back trajectories were initialised to connect the smoke to the fire at 1200 UTC.

during the Rim Fire and the Konza Prairie prescribed burns are in Peterson *et al.* (2015) and Whitehill *et al.* (2019), respectively. The PBL comparison of the observations with model STL showed that the model performed better for the Konza Prairie prescribed grassland burns (mean bias (MB) of  $\pm 400$  m) than for the Rim wildfire (MB of +1000 m; see S3, Planetary boundary layer (PBL) analysis).

*Remote sensing of plume heights  
Wildfire (Rim Fire)*

The 2013 California Rim Fire has been described as a massive wildfire, as the data here support. As of 2019, the

Rim Fire was California’s fifth largest wildfire. This was also a heavily actioned fire, which was fully contained 9 weeks after the fire ignition. CALIOP plume detrainment data are shown in Figs 3–5 and Table 4. Fig. 3 shows one of several CALIPSO curtains (see Fig. S1 for additional curtains and Fig. S2 for all tracks used), where smoke aerosol data were extracted to develop the daily smoke-plume detrainment height products (Fig. 5). Data were extracted from nine CALIPSO curtains to develop the daily smoke evolution for 21 August 2013 (Fig. 5), and seven curtains were extracted for 24 August 2013. Smoke-filled air parcels were injected and detrained into and above the PBL throughout the day on both 21 and 24 August, with plume

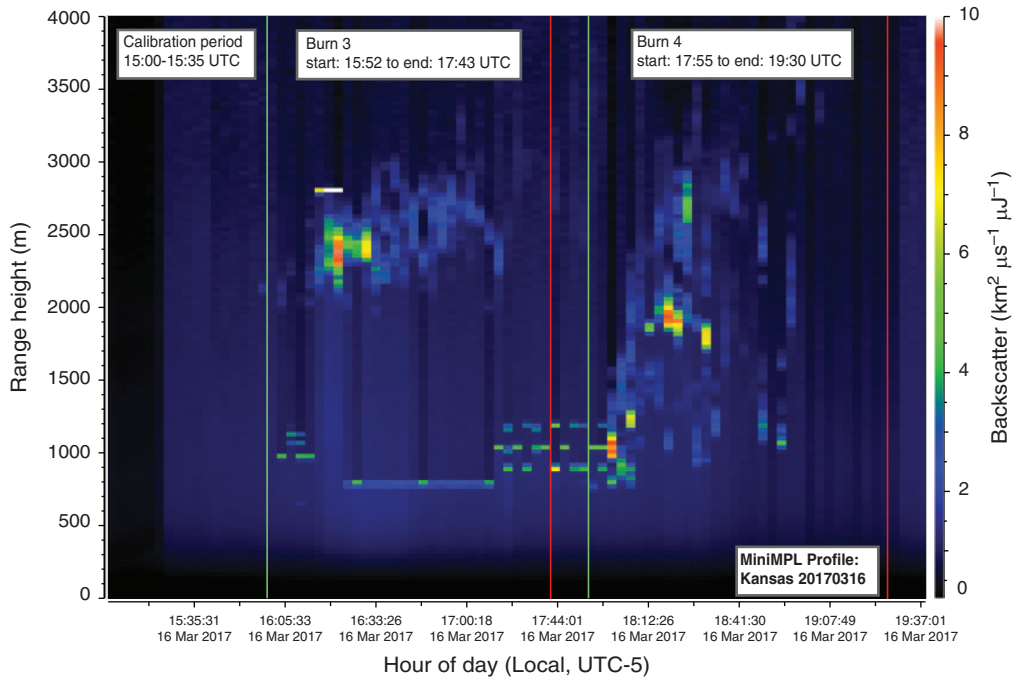


**Fig. 6.** 2017 Konza Prairie Biological Station prescribed burn experiment showing, for Burns 3 and 4 (16 March), smoke-plume range height (m above sea level) and backscatter ( $\text{km}^2 \mu\text{s}^{-1} \mu\text{J}^{-1}$ ), derived using a ground-based Hexagon Miniaturised Micro Pulse Lidar (MiniMPL). The lidar starting height was 440 m above sea level for the plume height measurements. For Burn 5 (20 March), see Fig. S5.

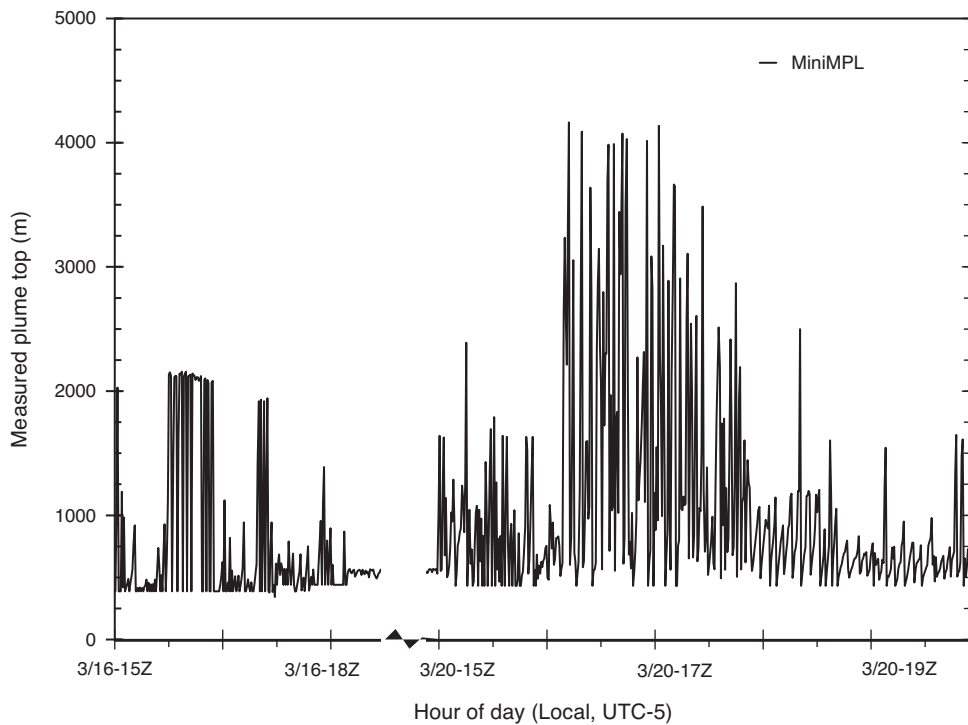


**Fig. 7.** 2017 Konza Prairie Biological Station prescribed burn experiment showing, for Burns 3 and 4 (16 March) and Burn 5 (20 March), maximum observed smoke plume tops (m above sea level), derived using a ground-based Hexagon Miniaturised Micro Pulse Lidar (MiniMPL). The lidar starting height was 440 m above sea level for the plume height measurements.

**Table 2. Plume rise model parameterisation**

Simulation name	Plume rise parameterisation
BASE12	CMAQ–Briggs simulation using a 12-h temporal profile (burn duration) at 12-km grid resolution with WRF (meteorological data)
BRIGGS12KMHR	Modified BASE12 using adjusted temporal profiles (3- or 4-h profile from the fire start time) at 12-km grid resolution
SOFIEV12KMHR	Modified CMAQ simulation using Sofiev to calculate plume rise with adjusted temporal profiles (3- or 4-h) at 12-km grid resolution
PBL50012KM	Modified CMAQ simulation using the model Planetary Boundary Layer plus a 500-m adjustment to set the plume top at 12-km grid resolution
BRIGGS4KMHR	Modified CMAQ–Briggs simulation using adjusted temporal profiles (12-, 4- or 3 h) at 4-km grid resolution
SOFIEV4KMHR	Modified CMAQ simulation using Sofiev to calculate plume rise with adjusted temporal profiles (12-, 4- or 3-h) at 4-km grid resolution
BRIGGS4KM12HR	CMAQ–Briggs simulations using a 12-h temporal profile at a 4-km grid resolution

heights increasing as the afternoon RH decreased and temperatures increased (Fig. 5).

The maximum FRP was much higher on 21 August (3025 MW; Fig. 5, Table 4), compared with that on 24 August (max. 1734 MW). The plume was injected over 1 km higher on 21 August from ~1500 local time throughout the day. On all days of the Rim Fire, 83% of the smoke was injected and detrained above the PBL (Table 4); 21 and 24 August were particularly active, with 92% of the smoke detrained above the PBL. The Rim Fire was intense, with much more smoke lofted higher in the atmosphere than is typical. This result contrasts with the larger-scale Multi-angle Imaging SpectroRadiometer (MISR) plume-height analysis (Val Martin *et al.* 2010), which showed that most smoke (88–96%) remained in the PBL, highlighting the differences in extreme fires compared with ‘normal’ fires. As a result, the standard 12-h assumption was retained.

#### *Prescribed fire (Konza Prairie burns)*

The scanning MiniMPL measurements (Fig. 6, Fig. S5) provide evidence that the largest smoke concentrations during the Konza burns were in the advancing portions of the fire. The lidar retrievals showed that smoke from these prairie fires <500 ha tended to pool in the lower PBL (Fig. 7, Table 1), with 17% entering the free troposphere. A comparison of the maximum PIH with the associated maximum backscatter concentrations indicates a contrasting pattern to the standard vertical fire emissions profile, which suggests that some of the smoke reached a higher elevation, but most pooled lower in the PBL. For example, with nearly triple the burn rate, Burn 5 had plumes nearly two to four times higher than Burns 3 and 4 (Fig. 7). For the individual fields <200 ha, smoke generally reached the top of the highest observed layer within the PBL, with some individual plume cores penetrating the PBL. This finding

verifies the capping potential of the PBL for prairie fires under these prevailing weather conditions.

The diurnal plume height and intensity from the Konza Prairie burns (Fig. 7) provides additional evidence that small fires (<500 ha) can penetrate the PBL, even if plumes are generated with short burn times (<1–4 h). Plume heights were measured at 600–4100 m, while the PBL range was 750–1270 m. These prescribed fires were consistent with other fires where the meteorological conditions constrained plume rise (e.g. capping inversion), but the burn rate played a lesser role (e.g. Burn 4 plume tops were, on average, 500 m higher than those of Burn 3, with a burn rate difference of only 32 ha h<sup>-1</sup>). The fuel loading for these fires showed no clear connection to PIH. For example, Burn 4 contained a fuel loading of 942 kg ha<sup>-1</sup> (~17%) more than Burn 3, but the resulting plume tops remained relatively similar.

On 20 March 2017, several fields totalling 405 ha burned concurrently in a small area relative to the AQM grid spacing; for this reason, we treated these as one field, Burn 5 (Fig. S5). Burn 5 produced several plumes with distinct cores that were injected 2000–3000 m above the PBL. Plumes that penetrated the PBL continued to rise to higher stable layers (3190 m at 1500–1700 UTC, 3750 m at 1800–2000 UTC). Still, a significant amount of the smoke remained just above the PBL (1300 m), which is consistent with smoke detraining at multiple levels in the atmosphere. Compared with Burn 5, the backscatter intensity of Burns 3 and 4 demonstrated that, as expected, plumes with a lower vertical extent had higher pollution concentrations near the surface.

#### *Model plume rise evaluation*

The plume rise evaluation was carried out on an hourly basis, for each model layer, and for each of the five burns we evaluated (Table 1). For the Rim Fire (Burns 1, 2), we used hourly averaged observational data from satellite-based retrievals from CALIOP (Fig. 8: maximum plume tops; Figs S3, S4: mean and minimum heights) to compare with each model formulation. For the Konza Prairie burns (Burns 3, 4, 5), we used hourly averaged ground-based retrievals from the MiniMPL (Figs 9–11).

#### *Model with Briggs plume rise evaluation: wildfire (Rim Fire)*

For the Rim Fire, the CMAQ–Briggs (BASE12) simulation overall demonstrated the ability to capture the mean PIH range observed (Fig. 8, lower end of the shaded area). The BASE12 simulation successfully captured plume ability from the Rim Fire to penetrate the PBL. The model–observations analysis with BASE12 consisted of an MB of less than ±5–20% compared with the alternative methods. The base simulation compared well with the 3000–5000-m mean plume height value range reported in Peterson *et al.* (2015). Compared with the observed and other PIH algorithms, BASE12 contained an inherent low bias of 1000 m during the day and a corresponding inherent high bias at night. The night-time plume height appeared to be mostly sporadic and only sometimes within the range of measurements. Similarly, Sofiev *et al.* (2013) stated that night-time plume height could not be substantiated because of the limited number of observations. These findings suggest that a high bias in particulate matter with a diameter smaller than

**Table 3. Plume rise model differences**

Approach	Briggs	Sofiev	PBL500
Type	Empirical, analytical	Empirical, analytical	Statistical
Scheme	Plume height is a function of downwind distance, modified for wildfire by Pouliot <i>et al.</i> (2005); plume top is calculated, and the plume bottom is set to be 2/3 of plume top value	Energy-balance-based parameterisation (similar to convective cloud formulations) accounting for planetary boundary layer (PBL) height, power law dependence of fire intensity, and stability above the PBL, with four fitted tuneable parameters to match observed plume heights by MISR	Observation-based, consistent statistical approximation
Input parameters	Area burned, fuel loading, wind speed, duration of fire, heat content, fire location coordinates	Fire Radiative Power (FRP), potential temperature as a function of geometric height to derive Brunt–Väisälä frequency, PBL height, fire location coordinates	PBL height, fire location coordinates
Output parameters	Top and bottom of smoke plume	Top of smoke plume	Top of smoke plume
Previous comparisons with satellite observations	Tendency to underpredict (Raffuse <i>et al.</i> 2012); plume tops are generally higher than Sofiev owing to inherent incompatibility and formulation (designed for stack heights), with fires (Sofiev <i>et al.</i> 2012)	Poor to moderate; comparable with or better than a one-dimensional plume rise model (Sofiev <i>et al.</i> 2012; Paugam <i>et al.</i> 2016)	Not available
Ease of implementation in CMAQ	Currently used	Low to moderate	Very low
Existing implementation	SMOKE, CMAQ, HYSPLIT	CMAQ (by Baldassarre <i>et al.</i> 2015)	Not currently used

**Table 4. Comparison of the percentage of smoke below and above the Planetary Boundary Layer (PBL) for the 2013 California Rim Fire (CALIOP data) and for the larger MISR analysis (Val Martin *et al.* 2010)**  
For the Rim Fire, most of the smoke was injected and detrained above the PBL

Data source	Air parcels	Max. plume height		Min. plume height	
	Number	% < PBL	% > PBL	% < PBL	% > PBL
Rim, 21 August	53 859	8	92	10	90
Rim, 24 August	96 965	8	92	28	72
Rim, total	601 291	17	83	36	64
MISR		88–96	4–12		

2.5  $\mu\text{m}$  ( $\text{PM}_{2.5}$ ), as discussed in Wilkins *et al.* (2018), could have been skewed by a night-time high bias in  $\text{PM}_{2.5}$  and not an overall daily model  $\text{PM}_{2.5}$  bias for wildfires.

#### *Model with sensitivities plume rise evaluation: wildfire (Rim Fire)*

Comparing the BASE12 run with the SOFIEV12KM12HR method provides additional evidence that BASE12 may underpredict PIH during the daytime for big spread events (12 068  $\text{ha day}^{-1}$ ) and overpredict PIH for moderate-spread events (6033  $\text{ha day}^{-1}$ ). The physical rationale method (PBL50012KM) determined that, during the day, PIH showed similar heights to CMAQ-Briggs, when the plume was constrained within the PBL (24 August). For times that the plume was not constrained within the PBL, the accuracy was limited by the height of the PBL. Our simulations did not couple meteorology and fire feedbacks as a system; therefore, we did not expect to capture fire emissions impacts to the PBL locally. This could include, but not be limited to, the impacts from fire heat

fluxes directly related to the fire and potential smoke radiative impacts on the PBL (e.g. Kochanski *et al.* 2019). If the system is not coupled, then this rationale may not be reasonable, because this method relies on plumes not escaping the PBL (e.g. Burn 2).

#### *Model with Briggs plume rise evaluation: prescribed fire (Konza Prairie)*

For the prescribed burns (Konza Prairie; Figs 9–11), the BASE12 simulation indicated an overall low PIH bias of 600–2000 m. According to the algorithm differences, the PBL50012KM performed better for the prescribed grassland burns than for the forested wildfire cases (Rim Fire). This difference suggests that the smaller grassland fires (<500 ha) had less impact on the boundary layer physics and contained fewer plumes that escaped the PBL (10–50%). Our results for PBL50012KM are consistent with conclusions from previous studies that when smoke is injected into the free troposphere, it tends to accumulate within atmospheric layers of relative stability aloft (Kahn *et al.* 2007; Val Martin *et al.* 2010).

#### *Model with sensitivities plume rise evaluation: prescribed fire (Konza Prairie)*

The Sofiev formulation most closely matched these observations. Therefore, we compared the performance of the Sofiev method with the CMAQ-Briggs (BASE12) method. This comparison provided more evidence that the BASE12 model is biased low (Burn 4: BASE12 MB –215.5 m, Sofiev MB –449.2; Burn 5: BASE12 MB –2975.1 m, Sofiev MB –3586.2 m). Lowering the grid spacing from 12 to 4 km provided little improvement in PIH estimates, only slightly increasing the error and bias. This small increase was likely because the meteorological input did not have many differences between the simulations (see S3, Planetary boundary layer (PBL) analysis).

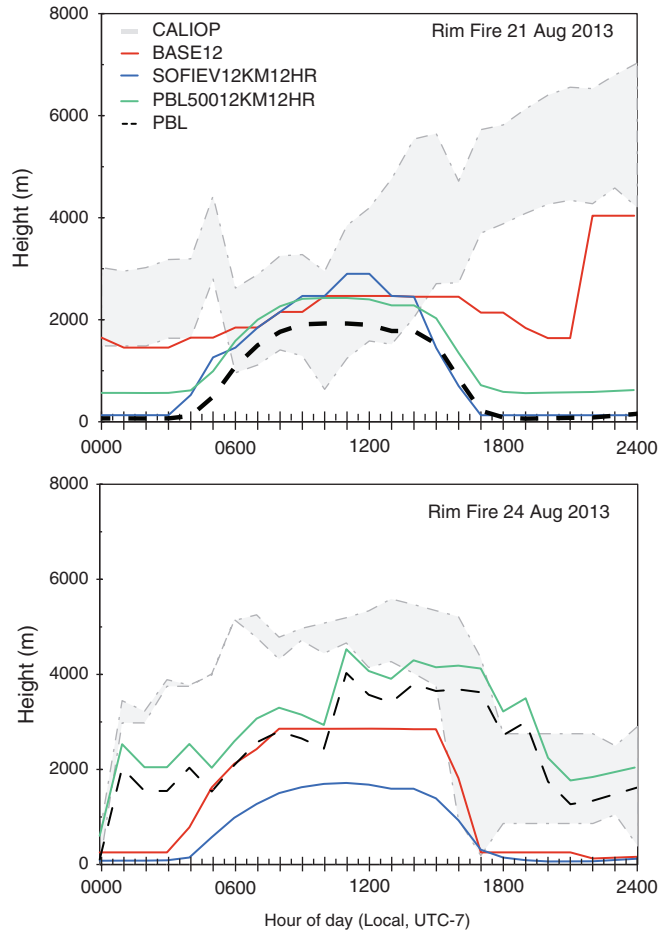


**Fig. 8.** 2013 California Rim Fire plume tops, derived from the CALIOP data (grey), CMAQ base model (red) with the planetary boundary layer (PBL, black dotted line), Sofiev method (blue), and PBL + 500 m approach (green). See Tables 2 and 3 for details on each simulation.

Lastly, using the updated temporal profile, 3–4 h compared with 12 h, the simulation switched the overall PIH estimation bias from negative to positive (e.g. for Burn 3, BASE12 MB –272.4 m; BRIGGS4KM MB 174.8 m). Furthermore, the model’s ability to simulate the overall maximum PIH improved by 200–1000 m. The difference in model performance for estimating PIH for Burns 3 and 4, compared with Burn 5, was because of model design and stability layers. However, CMAQ-Briggs is not designed to capture sharp rising plumes from small fires and rapid changes in the PBL, which typically cap vertical motion.

*Model to model plume rise: comparisons and bias*

Each model formulation (Table 2) was compared individually with the BASE12 simulation for the maximum PIH, the change in plume top compared with BASE12, and the percentage of plume change above PBL (Fig. 12). All simulations of plume top heights remained below 5000 m for the Rim wildfires and below 2000 m for the prescribed grassland burns at Konza. For the Rim Fire plume heights, a model-to-model comparison showed a 1500–2500-m high bias for both moderate and high-intensity burn days. For the prescribed grassland burns, there was a 50–1000-m low bias across all cases. For the wildfire cases, the base case placed >60% of the plume above the boundary layer, while

the other simulation placed 30–55% of the plume above the PBL. For grassland prescribed fires <500 ha, the base case placed <10% of the plume above the PBL, while the alternative model formulations placed 10–50% of the plume above the boundary layer, depending on area burned (e.g. Burn 5) and meteorological situation (e.g. Burn 4). The PBL50012KM simulation placed 50% of the plume above the PBL owing to the way the model was formulated. Therefore, after removing the PBL50012KM simulation, the actual average indicated that, for small fires, 10–35% of the smoke reached above the PBL.

*Model to observation plume height: comparisons and bias*

We evaluated the model bias against model formulation changes in plume rise algorithm, grid spacing and temporal allocation (Fig. 13). Overall, the BASE12 model had a consistent low bias of 10–3500 m for the Rim Fire burns. For estimating PIH, the standard base case model performed better (MB –2200 m, RMSE 3000 m) than all alternatives (MB –3500 m, RMSE 3500 m).

However, the base case model typically provided PIH estimates with the largest errors and bias for the Konza Prairie prescribed grassland burns. For fires <80 ha, BASE12 with 3–4-h implementation performed best. The model parameterised with Sofiev performed the best for all fires <500 ha, but by a

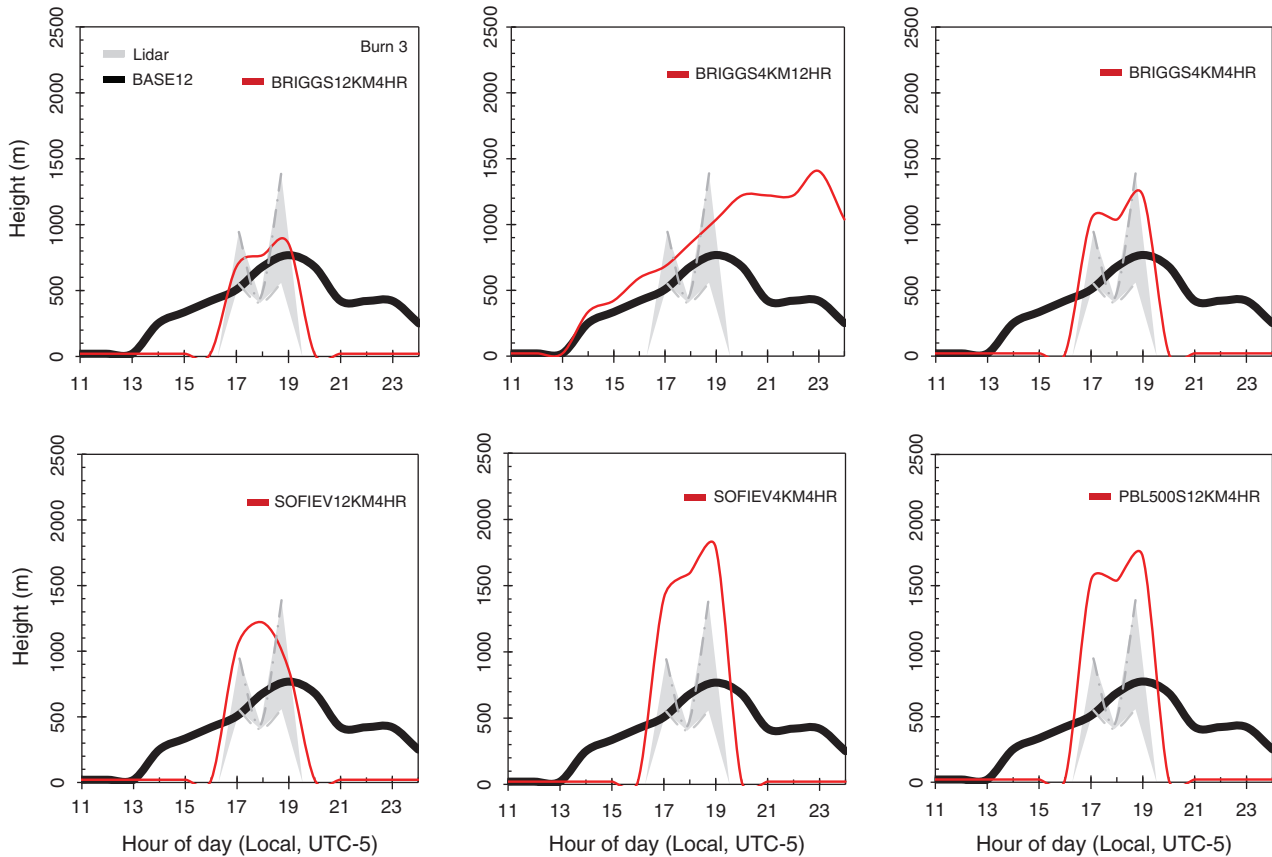


**Fig. 9.** Konza Burn 3 (16 March 2017): comparison of smoke plume tops for observed (grey), base model (black), and six model alternatives (red). See Tables 2 and 3 for model simulation configuration specifics.

relatively small margin (<400 m). The base model showed the most improvement when changing the temporal allocation (20–1000 m). There was negligible difference between the grid resolution choices (<300 m) owing to the model vertical grid sizes (20 to +500 m, increasing with height). A change lower than 500 m would not be significant computationally unless that model layer was near the PBL. More importantly, an error larger than 500 m could have placed smoke in the incorrect model vertical layer, leading to increased uncertainty in downwind transport (e.g. Burn 5).

## Discussion

### *Improving model performance due to plume rise*

The vertical extent of a wildland fire smoke plume is determined by its classification, detection and the fire inventory and modelling system. How a fire is classified or input into a model will determine how, or even if, a plume rise algorithm will be applied to a given fire. Generally, in most AQMs (e.g. CMAQ), only one numerical method is used to simulate plume rise for wildfires and prescribed fires. In some cases, smaller fires will not have adequate plume rise associated with their emissions (Zhou *et al.* 2018). With a limited sample size of fires, our results suggest that there are benefits to model performance by treating a fire event smoke plume rise with multiple formulations

selected based on the event's size, duration and type (wild or prescribed fire).

### *Night-time v. daytime plume rise*

For large wildland fires, night-time *v.* daytime plume rise proved to be an area of concern (Sofiev *et al.* 2013). The night-time high bias in BASE12-estimated plume height might have been due to missing night-time fire characteristics (e.g. model physics, meteorology, intensity, detection). The Burn 2 simulation in the Rim Fire revealed a higher plume height bias during the daytime and a low night-time bias comparable with Sofiev's method (potentially due to the heat flux value from BlueSky near zero). Furthermore, the heat flux input from the BlueSky framework, although loosely correlated with satellite-derived FRP, tends to underestimate injection height (Kahn *et al.* 2007; Val Martin *et al.* 2010, 2012). This may occur if (i) satellite pixels of the order of 1 km<sup>2</sup> are only partly filled with a fire (Giglio *et al.* 2006); (ii) there is overlying smoke opacity (Kahn *et al.* 2008); or (iii) fire elements have non-unit emissivity, such as smouldering fractions (Val Martin *et al.* 2018). The suggested solution has been for modellers to multiply heat flux by a factor of 5 or more to match true plume buoyancy (Kahn *et al.* 2007; Ichoku and Ellison 2014). However, applying this adjustment here did not improve either simulation.

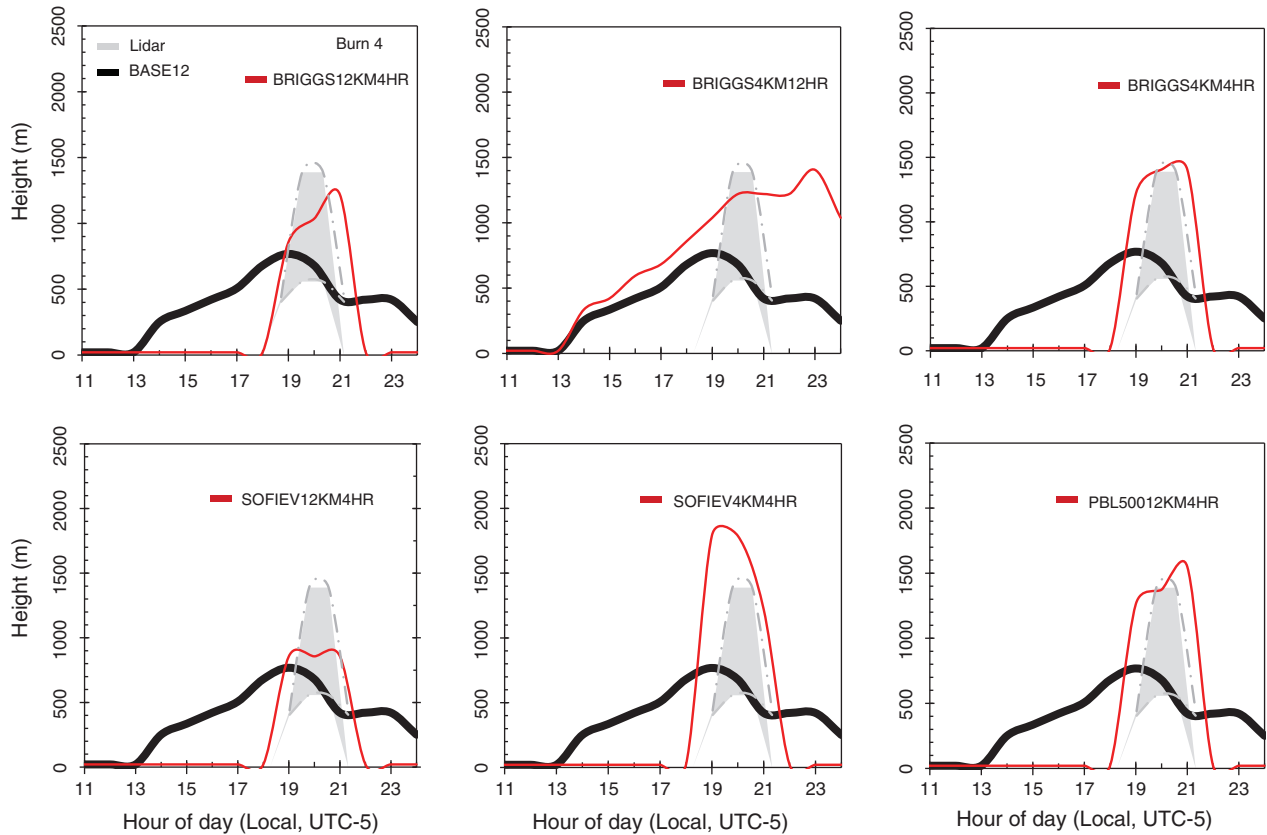


**Fig. 10.** Konza Burn 4 (16 March 2017): comparison of smoke plume tops for observed (grey), base model (black), and six model alternatives (red). See Tables 2 and 3 for model simulation configuration specifics.

Another concern is that lingering smoke may be captured by observations but missed or ventilated out in model simulations. A full analysis of night-time plume rise for this study was not possible, because no fire observations were taken at night. Another difference between observation and models related to large wildland fires concerned the area burned. For example, plumes from Burns 1 and 2 produced significantly different average observed plume heights (4000–6000-m differences), but model simulations remained similar, in the range of 2000–3000 m. To improve the validation method for modelling, the use of the Soja *et al.* (2009, 2012) satellite-based method was helpful, because the plume tops derived were within 500–1000 m of those Peterson *et al.* (2015) and Saide *et al.* (2015) reported from the same fire.

#### Temporal allocation – burn duration

For the Konza Prairie small prescribed grassland fires (<500 ha), selecting the proper temporal allocation of emissions and heat fluxes was even more critical than the actual algorithm. For the Rim Fire or larger fires (>5000 to 10 000 ha per day) that do not follow the typical diurnal cycle within an AQMs' temporal profile, we suggest that it can be better to obtain hourly burned area from, e.g. Geostationary Operational Environmental Satellite (GOES), to estimate fire emissions. Model performance here improved with temporal allocation based on hourly observations but there is potential for greater improvement with the use of a proper treatment of sub-hourly fluctuations. When emissions

were allocated based on size of fire and active burning phase, model performance improved significantly (+1000 m). Moreover, there was a connection between model plume heights and stability layers, consistent with earlier studies (e.g. Val Martin *et al.* 2018). Smoke pooled in stability layers. The stability layer in which a plume would be capped was determined by the strength of that stability layer compared with the energy or lift of an individual plume or buoyancy, a measure of stability calculated as buoyancy frequency. Burn 5 exhibits evidence for the importance of these layers, where plumes that penetrated the PBL continued vertically until reaching the next stable layer at ~3000 m.

Evaluating ways to improve the performance of contemporary AQMs should focus on providing numerically efficient algorithm choices and readily available supplementary data streams. To advance our understanding of smoke dispersion events, the model user should be allowed to select (i) plume rise algorithms based on fire type, and (ii) the time constraints and emission allocation windows. Based on this study, we suggest the following modelling improvements: (i) provide the option to use 4–6 h emissions allocation windows based on the fuel loading and field size, instead of 11 h from the detection time; (ii) if the fire start time is unknown, use the time of fire detection and place the time profile before and after the detection hour (e.g. for a fire detected at 1100 UTC, time profile would be 0900–1300 UTC); (iii) provide for the use of region-specific information such as weather, fuels and burn practices, because these results were highly reflective of the Flint

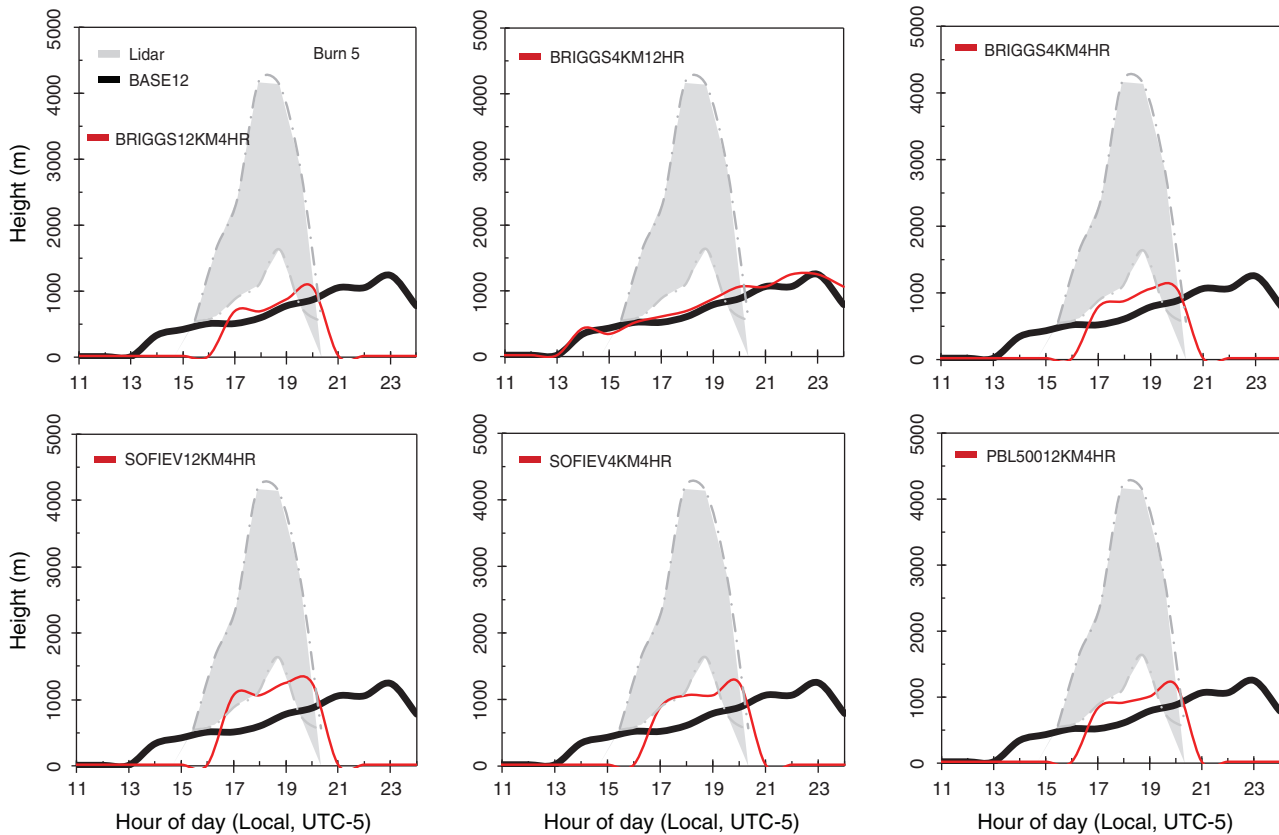


**Fig. 11.** Konza Burn 5 (20 March 2017); comparison of smoke plume tops for observed (grey), base model (black), and six model alternatives (red). See Tables 2 and 3 for model simulation configuration specifics.

Hills environment and associated fuels (grassland fields) of the Konza Prairie prescribed burn; (iv) allow for variable burn rates, because we found that the optimum estimates for intense to mildly intense fire spread rates were 20–35 ha h<sup>-1</sup> for the Flint Hills region, in contrast to 250–500 ha h<sup>-1</sup> for the Rim Fire.

## Conclusions

Smoke plume injection height (PIH) is an important predictor of how smoke is transported and dispersed downwind of a wildland fire. Most air quality models rely on plume rise methods to determine the vertical allocation of emissions. In this study, we compared several methods with observed PIH. We used the CMAQ modelling system to investigate the impacts of model grid spacing, emissions temporal profile and three plume rise algorithms for five burn events (two wildfire and three prescribed).

Although approaches more advanced than the Briggs algorithm offer the potential to incorporate complex features of wildland fires, our results indicate that the Briggs algorithm performed comparably when provided improved inputs (MB of less than  $\pm 5$ –20% and RMSE lower than 1000 m compared with the alternatives). Our results indicate that the standard model formulation for plume rise has a high bias for large fires (MB range of 1000 to 3000 m). This high bias could be due to a high night-time bias, since the model had a pervasive low daytime bias. Predictions of PIH rely on correctly determining

the PBL height. For prescribed grassland burns, the maximum PIH using all approaches was largely underpredicted. However, the bias and mean error, MB of 200 to 600 m and RMSE of 600 to 2000 m, were improved with a more resolved temporal profile (3 to 4 h compared with 12 h). Lastly, the assumption that a rising smoke plume will tend to rest near an STL is valid, but the onus is on the model's ability to accurately capture those layers. For the large wildfire case (Rim Fire), Briggs placed >60% of the plume above the boundary layer, compared with 83% from observations and 30–55% from alternative models. For the Konza Prairie grassland prescribed fires <500 ha, the Briggs model placed <10% of the plume above the PBL, compared with 17% from observations and 10–35% from alternatives. Thus, the Briggs model performs better if not comparably for wildfires compared with the alternatives while for prescribed fires, Briggs requires adjustments to improve performance.

Based on these findings, we suggest the following modifications to the current air quality modelling system:

- Compute plume rise for small fires (<500 ha). Many current models simply inject smoke from small fires into the boundary layer or the lowest model layer.
- Assume a temporal profile that more closely matches the active burn period of a prescribed fire. Many models currently assume 12 or 24 h, but this tends to dilute the emissions and heat intensity of these fires.

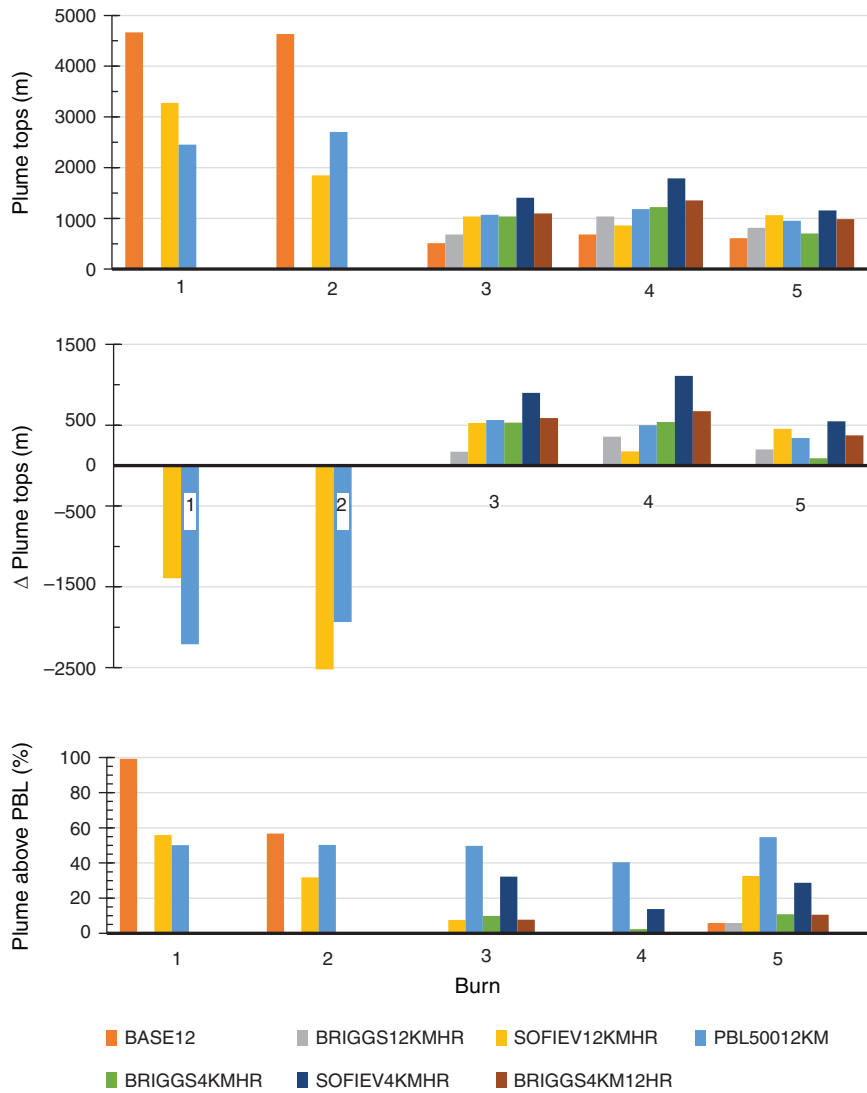


**Fig. 12.** Modelled plume information is shown for each of the five burns selected at the 2013 California Rim Fire (Burns 1, 2) and the 2017 Konza Prairie prescribed burn (Burns 3, 4, 5). Orange: BASE12, grey: BRIGGS12KMHR, yellow: SOFIEV12KMHR, light blue: PBL50012KM, green: BRIGGS4KMHR, dark blue: SOFIEV4KMHR, brown: BRIGGS4KM12HR. Top: Plume tops (above ground level) for each simulation. Middle: change in plume tops compared with BASE12. Bottom: percentage of the plume above the planetary boundary layer (PBL).

- Assume a fire-specific temporal profile, and if information is not available, apply one of two selectable options:
  - Take the detection time and generate a temporal profile (e.g. if fire is detected by MODIS or GOES-16/17 at 1100 UTC, time profile applied if using 4 h will be 0900–1300 UTC for the burn).
  - Use the burn rate or the regional average estimate of area burned (e.g. 35 ha h<sup>-1</sup> for the Konza Prairie prescribed burn).

Information on wild and prescribed fire is limited. Therefore, a lack of data persists as an inherent limitation of our study, which only considered the use of a small sample size of fires. But the resulting smoke emissions and impacts are substantial and clear enough to extrapolate relevant findings

for future recommendations. Given the findings of this study, we suggest providing a temporal allocation tailored to the types of fires presented. To help with this matter, we urge and suggest that forest agencies, fire land managers and others collect information or create a survey of burn practices by region, season and type of biomass, as indicated in Section 7 of the US EPA National Emissions Inventory documentation (US EPA 2018). Fire plume rise modelling can be improved with the incorporation of space-based retrievals (Soja *et al.* 2012; Val Martin *et al.* 2018; Sokolik *et al.* 2019), databases for plume heights that are not typically modelled (e.g. intense pyrocumulonimbus: Lareau and Clements 2016; Peterson *et al.* 2017; Wilkins *et al.* 2020), ground-based measurements (Clements *et al.* 2018) and fuel consumption rate assessments (van

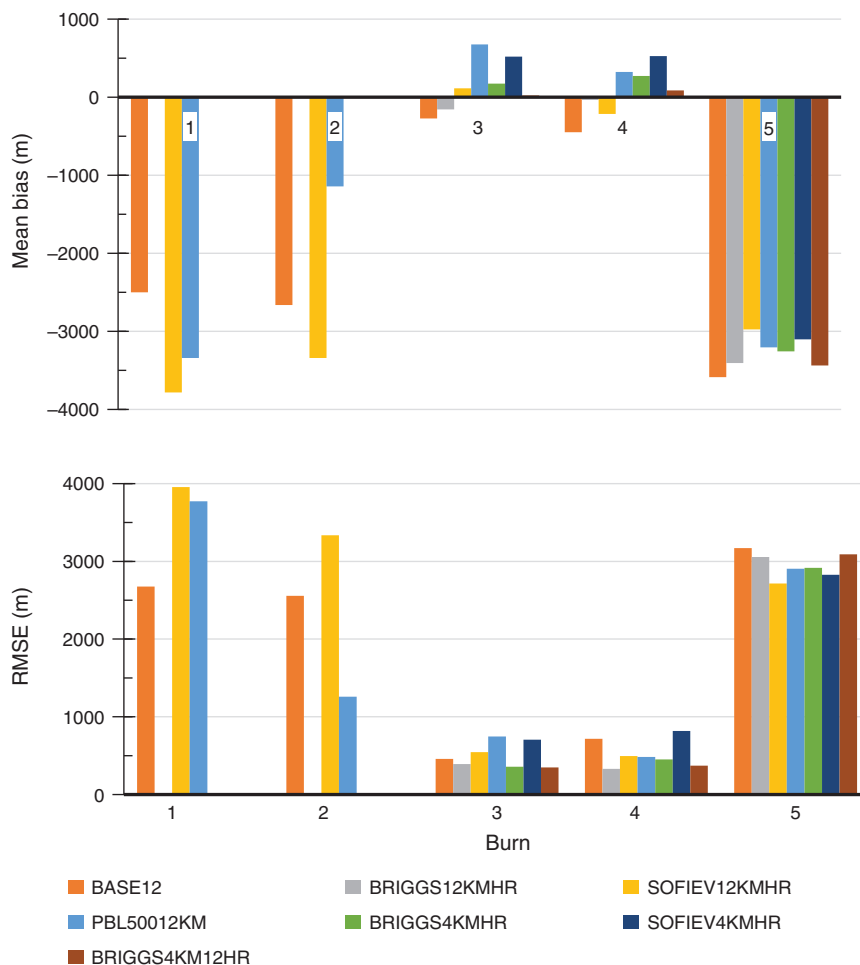


**Fig. 13.** Modelled plume information is shown for each of the five burns selected at the 2013 California Rim Fire (Burns 1, 2) and the 2017 Konza Prairie prescribed burn (Burns 3, 4, 5). Orange: BASE12, grey: BRIGGS12KMHR, yellow: SOFIEV12KMHR, light blue: PBL50012KM, green: BRIGGS4KMHR, dark blue: SOFIEV4KMHR, brown: BRIGGS4KM12HR. Top: mean bias (MB) for each simulation. Bottom: root mean square error (RMSE) change in plume tops compared with the observations.

Leeuwen *et al.* 2014). We recommend that future research explore the potential benefits of a hybrid approach combining multiple algorithms that can be used interchangeably based on conditions encountered by the model. For example, Wilkins *et al.* (2020) demonstrated a potential for increase in local ozone by 10–80 ppbv downwind of major biomass-burning sources. Plume rise algorithms are not limited to those presented here; in the future, we seek to investigate other methodologies, e.g. the 1-D model of Freitas *et al.* (2007), in order to evaluate them against observations. Lastly, we suggest an enhanced analysis of the impact of meteorological inputs on plume rise models, which could improve information available to prescribed burn decision-makers (e.g. burn windows, plume dispersion height and direction). These suggested improvements could help enable near-real time model predictions for fire modelling (Marsha and Larkin 2019; Shankar *et al.* 2019).

### Conflicts of interest

The authors declare that they have no conflicts of interest.

### Declaration of funding

This research did not receive any specific funding. We are greatly appreciative of NASA funding for the CALIPSO work from the CloudSat and CALIPSO Science Team under grant number NNX16AM30G.

### Acknowledgements

The views expressed in this paper are those of the authors and do not necessarily reflect the views or policies of the US EPA. Mention of trade names or commercial products does not constitute an endorsement or recommendation for use. We thank Kansas State University, Nature Conservancy, Konza Prairie Biological Station staff, Micro Pulse LiDAR, part of Hexagon staff, Jacky Rosati-Rowe, Shawn Roselle, Brian Gullet, James Szykman and Russell Long (EPA Office of Research and Development), Andrew Habel (Jacobs Technology, Inc.). Special thanks to Homaira Sharif and Randa Boykin for their graphical assistance. We thank Kirk Baker for assisting with lidar daily operations and Patricia Loesche for editorial comments. Lastly, a special thanks and dedication to the life of Eliza Bradford.

## References

- Achtmeier GL, Goodrick SA, Liu YQ, Garcia-Menendez F, Hu YT, Odman MT (2011) Modeling smoke plume-rise and dispersion from southern United States prescribed burns with daysmoke. *Atmosphere* **2**, 358–388. doi:10.3390/ATMOS2030358
- Al-Saadi J, Soja AJ, Pierce RB, Szykman J, Wiedinmyer C, Emmons L, Kondragunta S, Zhang X, Kittaka C, Schaack T, Bowman K (2008) Intercomparison of near-real-time biomass burning emissions estimates constrained by satellite fire data. *Journal of Applied Remote Sensing* **2**, 021504. doi:10.1117/1.2948785
- Andreae MO, Merlet P (2001) Emission of trace gases and aerosols from biomass burning. *Global Biogeochemical Cycles* **15**, 955–966. doi:10.1029/2000GB001382
- Baker K, Woody M, Valin L, Szykman J, Yates E, Iraci L, Choi H, Soja A, Koplitz S, Zhou L (2018) Photochemical model evaluation of 2013 California wildfire air quality impacts using surface, aircraft, and satellite data. *The Science of the Total Environment* **637–638**, 1137–1149. doi:10.1016/J.SCITOTENV.2018.05.048
- Baker K, Koplitz S, Foley KM, Hawkins A (2019) Characterizing grassland fire activity in the Flint Hills region and air quality using satellite and routine surface monitor data. *The Science of the Total Environment* **659**, 1555–1566. doi:10.1016/J.SCITOTENV.2018.12.427
- Baldassarre G, Pozzoli L, Schmidt CC, Unal A, Kindap T, Menzel WP, Whitburn S, Coheur PF, Kavgaci A, Kaiser JW (2015) Using SEVIRI fire observations to drive smoke plumes in the CMAQ air quality model: a case study over Antalya in 2008. *Atmospheric Chemistry and Physics* **15**, 8539–8558. doi:10.5194/ACP-15-8539-2015
- Briggs GA (1975) Plume rise predictions. In 'Lectures on air pollution and environmental impact analyses'. (Ed. Haugen D) pp. 59–111 (American Meteorological Society: Boston, MA, USA).
- Charland AM, Clements CB (2013) Kinematic structure of a wildland fire plume observed by Doppler lidar. *Journal of Geophysical Research, D, Atmospheres* **118**, 3200–3212. doi:10.1002/JGRD.50308
- Clements CB, Oliphant AJ (2014) The California State University mobile atmospheric profiling system: a facility for research and education in boundary layer meteorology. *Bulletin of the American Meteorological Society* **95**, 1713–1724. doi:10.1175/BAMS-D-13-00179.1
- Clements CB, Potter BE, Zhong S (2006) In situ measurements of water vapor, heat and CO<sub>2</sub> fluxes within a prescribed grass fire. *International Journal of Wildland Fire* **15**, 299–306. doi:10.1071/WF05101
- Clements CB, Zhong S, Goodrick S, Li J, Bian X, Potter BE, Heilman WE, Charney JJ, Perna R, Jang M, Lee D, Patel M, Street S, Aumann G (2007) Observing the dynamics of wildland grass fires: FireFlux – a field validation experiment. *Bulletin of the American Meteorological Society* **88**, 1369–1382. doi:10.1175/BAMS-88-9-1369
- Clements CB, Lareau NP, Seto D, Contezac J, Davis B, Teske C, Zajkowski TJ, Hudak AT, Bright BC, Dickinson MB, Butler BW, Jimenez D, Hiers JK (2016) Fire weather conditions and fire-atmosphere interactions observed during low-intensity prescribed fires – RxCADRE 2012. *International Journal of Wildland Fire* **25**, 90–101. doi:10.1071/WF14173
- Clements CB, Lareau NP, Kingsmill DE, Bowers CL, Camacho CP, Bagley R, Davis B (2018) The Rapid Deployments to Wildfires Experiment (RaDFIRE): observations from the fire zone. *Bulletin of the American Meteorological Society* **99**, 2539–2559. doi:10.1175/BAMS-D-17-0230.1
- Colarco PR, Schoeberl MR, Doddridge BG, Marufu LT, Torres O, Welton EJ (2004) Transport of smoke from Canadian forest fires to the surface near Washington, DC: injection height, entrainment, and optical properties. *Journal of Geophysical Research* **109**, D06203. doi:10.1029/2003JD004248
- Fann N, Alman B, Broome RA, Morgan GG, Johnston FH, Pouliot G, Rappold AG (2018) The health impacts and economic value of wildland fire episodes in the US: 2008–2012. *The Science of the Total Environment* **610–611**, 802–809. doi:10.1016/J.SCITOTENV.2017.08.024
- Freitas SR, Longo KM, Andreae MO (2006) Impact of including the plume rise of vegetation fires in numerical simulations of associated atmospheric pollutants. *Geophysical Research Letters* **33**, L17808. doi:10.1029/2006GL026608
- Freitas SR, Longo KM, Chatfield R, Latham D, Silva Dias MAF, Andreae MO, Prins E, Santos JC, Gielow R, Carvalho Jr JA (2007) Including the sub-grid scale plume rise of vegetation fires in low resolution atmospheric transport models. *Atmospheric Chemistry and Physics* **7**, 3385–3398. doi:10.5194/ACP-7-3385-2007
- Gelaro R, McCarty W, Suárez MJ, et al. (2017) The Modern-Era Retrospective Analysis for Research and Applications, Version 2 (MERRA-2). *Journal of Climate* **30**, 5419–5454. doi:10.1175/JCLI-D-16-0758.1
- Giglio L, Descloitres J, Justice CO, Kaufman YJ (2003) An enhanced contextual fire detection algorithm for MODIS. *Remote Sensing of Environment* **87**, 273–282. doi:10.1016/S0034-4257(03)00184-6
- Giglio L, Van der Werf G, Randerson J, Collatz G, Kasibhatla P (2006) Global estimation of burned area using MODIS active fire observations. *Atmospheric Chemistry and Physics* **6**, 957–974. doi:10.5194/ACP-6-957-2006
- Giglio L, Randerson JT, van der Werf GR, Kasibhatla PS, Collatz GJ, Morton DC, DeFries RS (2010) Assessing variability and long-term trends in burned area by merging multiple satellite fire products. *Biogeosciences* **7**, 1171–1186. doi:10.5194/BG-7-1171-2010
- Goodrick SL, Achtmeier GL, Larkin NK, Liu Y, Strand TM (2013) Modelling smoke transport from wildland fires: a review *International Journal of Wildland Fire* **22**, 83–94. doi:10.1071/WF11116
- Gordon M, Makar PA, Staebler RM, Zhang J, Akingunola A, Gong W, Li S-M (2018) A comparison of plume rise algorithms to stack plume measurements in the Athabasca oil sands. *Atmospheric Chemistry and Physics* **18**, 14695–14714. doi:10.5194/ACP-18-14695-2018
- Hyer EJ, Allen DJ, Kasischke ES (2007) Examining injection properties of boreal forest fires using surface and satellite measurements of CO transport. *Journal of Geophysical Research* **112**, D18307. doi:10.1029/2006JD008232
- Ichoku C, Ellison L (2014) Global top-down smoke-aerosol emissions estimation using satellite fire radiative power measurements. *Atmospheric Chemistry and Physics* **14**, 6643–6667. doi:10.5194/ACP-14-6643-2014
- Ichoku C, Kahn R, Chin M (2012) Satellite contributions to the quantitative characterization of biomass burning for climate modelling. *Atmospheric Research* **111**, 1–28. doi:10.1016/J.ATMOSRES.2012.03.007
- Johnston FH, Henderson SB, Chen Y, Randerson JT, Marlier M, Defries RS, Kinney P, Bowman DM, Brauer M (2012) Estimated global mortality attributable to smoke from landscape fires. *Environmental Health Perspectives* **120**, 695–701. doi:10.1289/EHP.1104422
- Kahn RA, Li WH, Moroney C, Diner DJ, Martonchik JV, Fishbein E (2007) Aerosol source plume physical characteristics from space-based multi angle imaging. *Journal of Geophysical Research, D, Atmospheres* **112**, D11205. doi:10.1029/2006JD007647
- Kahn RA, Chen Y, Nelson DL, Leung FY, Li Q, Diner DJ, Logan JA (2008) Wildfire smoke injection heights: Two perspectives from space. *Geophysical Research Letters* **35**, L04809. doi:10.1029/2007GL032165
- Kochanski AK, Mallia DV, Fearon MG, Mandel J, Souril AH, Brown T (2019) Modeling wildfire smoke feedback mechanisms using a coupled fire-atmosphere model with a radiatively active aerosol scheme. *Journal of Geophysical Research, D, Atmospheres* **124**, 9099–9116. doi:10.1029/2019JD030558
- Kovalev VS, Newton J, Wold C, Hao WM (2005) Simple algorithm to determine the near-edge smoke boundaries with scanning lidar. *Applied Optics* **44**, 1761–1768. doi:10.1364/AO.44.001761

- Labonne M, Bréon F-M, Chevallier F (2007) Injection height of biomass burning aerosols as seen from a spaceborne lidar. *Geophysical Research Letters* **34**, L11806. doi:10.1029/2007GL029311
- Lareau NP, Clements CB (2016) Environmental controls on pyrocumululus and pyrocumulonimbus initiation and development. *Atmospheric Chemistry and Physics* **16**, 4005–4022. doi:10.5194/ACP-16-4005-2016
- Larkin NK, O'Neill SM, Solomon R, Raffuse S, Strand T, Sullivan DC, Ferguson SA (2009) The BlueSky smoke modeling framework. *International Journal of Wildland Fire* **18**, 906–920. doi:10.1071/WF07086
- Lelieveld J, Evans JS, Fnais M, Giannadaki D, Pozzer A (2015) The contribution of outdoor air pollution sources to premature mortality on a global scale. *Nature* **525**, 367–371. doi:10.1038/NATURE15371
- Leung F-YT, Logan JA, Park R, Hyer E, Kasischke E, Streets D, Yurganov L (2007) Impacts of enhanced biomass burning in the boreal forests in 1998 on tropospheric chemistry and the sensitivity of model results to the injection height of emissions. *Journal of Geophysical Research* **112**, D10313. doi:10.1029/2006JD008132
- Liu Y-Q, Goodrick S, Achtemeier G, Forbus K, Combs D (2013) Smoke plume height measurement of prescribed burns in the southeastern United States. *International Journal of Wildland Fire* **22**, 130–147. doi:10.1071/WF11072
- Liu Y, Kochanski A, Baker KR, Mell W, Linn R, Paugam R, Mandel J, Fournier A, Jenkins MA, Goodrick S, Achtemeier G, Zhao F, Ottmar R, French NHF, Larkin N, Brown T, Hudak A, Dickinson M, Potter B, Clements C, Urbanski S, Prichard S, Watts A, McNamara D (2019) Fire behaviour and smoke modelling: model improvement and measurement needs for next-generation smoke research and forecasting systems. *International Journal Wildland Fire* **28**, 570–588. doi:10.1071/WF18204
- Mallia DV, Kochanski AK, Urbanski SP, Lin JC (2018) Optimizing smoke and plume rise modeling approaches at local scales. *Atmosphere* **9**, 166. doi:10.3390/ATMOS9050166
- Marsha A, Larkin NK (2019) A statistical model for predicting PM<sub>2.5</sub> for the western United States. *Journal of the Air & Waste Management Association* **69**, 1215–1229. doi:10.1080/10962247.2019.1640808
- McCarthy N, McGowan H, Guyot A, Dowdy A (2018) MOBILE X-POL RADAR: A new tool for investigating pyroconvection and associated wildfire meteorology. *Bulletin of the American Meteorological Society* **99**, 1177–1195. doi:10.1175/BAMS-D-16-0118.1
- McKendry IG, van der Kampa D, Strawbridge KB, Christen A, Crawford B (2009) Simultaneous observations of boundary layer aerosol layers with CL31 ceilometer and 1064/532 nm lidar. *Atmospheric Environment* **43**, 5847–5852. doi:10.1016/J.ATMOSNV.2009.07.063
- McKendry IG, Gallagher J, Campuzano P, Bertram A, Strawbridge K, Leitch R, Macdonald AM (2010) Ground-based remote sensing of an elevated forest fire aerosol layer. *Atmospheric Chemistry and Physics* **10**, 11-921–11-930. doi:10.5194/ACP-10-11921-2010
- McKenzie D, Raymond CL, Kellogg L-KB, Norheim RA, Andreu AG, Bayard AC, Kopper KE, Elman E (2007) Mapping fuels at multiple scales: landscape application of the Fuel Characteristic Classification System. *Canadian Journal of Forest Research* **37**, 2421–2437. doi:10.1139/X07-056
- Mims SR, Kahn RA, Moroney CM, Gaitley BJ, Nelson DL, Garay MJ (2010) MISR stereo heights of grassland fire smoke plumes in Australia. *IEEE Transactions on Geoscience and Remote Sensing* **48**, 25–35. doi:10.1109/TGRS.2009.2027114
- Münkel C, Eresmaa N, Räsänen J, Karppinen A (2007) Retrieval of mixing height and dust concentration with lidar ceilometers. *Boundary-Layer Meteorology* **124**, 117–128. doi:10.1007/S10546-006-9103-3
- Omar AH, Winker DM, Vaughan MA, Hu Y, Trepte CR, Ferrare RA, Lee K-P, Hostetler CA, Kittaka C, Rogers RR, Kuehn RE, Liu Z (2009) The Calipso Automated Aerosol Classification and Lidar Ratio selection algorithm. *Journal of Atmospheric and Oceanic Technology* **26**, 1994–2014. doi:10.1175/2009JTECHA1231.1
- Ottmar RD, Sandberg DV, Riccardi CL, Prichard SJ (2007) An overview of the fuel characteristic classification system – quantifying, classifying, and creating fuelbeds for resource planning. *Canadian Journal of Forest Research* **37**, 2383–2393. doi:10.1139/X07-077
- Paugam R, Wooster M, Freitas S, Val Martin M (2016) A review of approaches to estimate wildfire plume injection height within large-scale atmospheric chemical transport models. *Atmospheric Chemistry and Physics* **16**, 907–925. doi:10.5194/ACP-16-907-2016
- Peterson DA, Hyer EJ, Campbell JR, Fromm MD, Hair JW, Butler CF, Fenn MA (2015) The 2013 Rim Fire: Implications for predicting extreme fire spread, pyroconvection, and smoke emissions. *Bulletin of the American Meteorological Society* **96**, 229–247. doi:10.1175/BAMS-D-14-00060.1
- Peterson DA, Hyer EJ, Campbell JR, Solbrig JE, Fromm MD (2017) A conceptual model for development of intense pyrocumulonimbus in western North America. *Monthly Weather Review* **145**, 2235–2255. doi:10.1175/MWR-D-16-0232.1
- Peterson DA, Campbell J, Hyer E, Fromm M, Kablick G, Cossuth J, DeLand M (2018) Wildfire-driven thunderstorms cause a volcano-like stratospheric injection of smoke. *NPJ Climate and Atmospheric Science* **1**, 30. doi:10.1038/S41612-018-0039-3
- Pierce RB, Al-Saadi JA, Schaack T, *et al.* (2003) Regional Air Quality Modeling System (RAQMS) predictions of the tropospheric ozone budget over east Asia. *Journal of Geophysical Research* **108**, 8825. doi:10.1029/2002JD003176
- Pierce RB, Al-Saadi J, Kittaka C, *et al.* (2009) Impacts of background ozone production on Houston and Dallas, Texas, air quality during the Second Texas Air Quality Study field mission. *Journal of Geophysical Research - Atmospheres* **114**, D00F09. doi:10.1029/2008JD011337
- Pouliot G, Pierce T, Benjey W, O'Neill SM, Ferguson SA (2005) Wildfire emission modeling: integrating BlueSky and SMOKE. In '14th Annual International Emission Inventory Conference', 11–14 April 2005, Las Vegas, NV. (US Environmental Protection Agency: Research Triangle Park, NC) Available at <http://www.epa.gov/ttn/chief/conference/ei14/session12/pouliot.pdf> [Verified 25 August 2018].
- Raffuse S, Wade K, Stone J, Sullivan D, Larkin N, Strand T, Solomon R (2009) Validation of modeled smoke plume injection heights using satellite data. In 'Eighth Symposium on Fire and Forest Meteorology', 12–15 October 2009, Kalispell, MT.
- Raffuse SM, Craig KJ, Larkin NK, Strand TT, Sullivan DC, Wheeler NJM, Solomon R (2012) An evaluation of modeled plume injection height with satellite-derived observed plume height. *Atmosphere* **3**, 103–123. doi:10.3390/ATMOS3010103
- Rappold AG, Reyes J, Pouliot G, Cascio WE, Diaz-Sanchez D (2017) Community vulnerability to health impacts of wildland fire smoke exposure. *Environmental Science & Technology* **51**, 6674–6682. doi:10.1021/ACS.EST.6B06200
- Rio C, Hourdin F, Chédin A (2010) Numerical simulation of tropospheric injection of biomass burning products by pyro-thermal plumes. *Atmospheric Chemistry and Physics* **10**, 3463–3478. doi:10.5194/ACP-10-3463-2010
- Saïde PE, Peterson DA, da Silva A, Anderson B, Ziemba LD, Diskin G, Sachse GW, Hair JW, Butler CF, Fenn ME, Jimenez JL, Campuzano-Jost P, Perring AE, Schwarz JP, Markovic MZ, Russell P, Redemann J, Shinzuka Y, Streets DG, Yan F, Dibb JE, Yokelson RJ, Toon OB, Hyer E, Carmichael GR (2015) Revealing important nocturnal and day-to-day variations in fire smoke emissions through a multiplatform inversion. *Geophysical Research Letters* **42**, 3609–3618. doi:10.1002/2015GL063737
- Shankar U, McKenzie D, Prestemon JP, Baek BH, Omary M, Yang D, Xiu A, Talgo K, Vizuete W (2019) Evaluating wildfire emissions projection methods in comparisons of simulated and observed air quality. *Atmospheric Chemistry and Physics* **19**, 15157–15181. doi:10.5194/ACP-19-15157-2019

- Sofiev M, Ermakova T, Vankevich R (2012) Evaluation of the smoke injection height from wildland fires using remote-sensing data. *Atmospheric Chemistry and Physics* **12**, 1995–2006. doi:10.5194/ACP-12-1995-2012
- Sofiev M, Vankevich R, Ermakova T, Hakkarainen J (2013) Global mapping of maximum emission heights and resulting vertical profiles of wildfire emissions. *Atmospheric Chemistry and Physics* **13**, 7039–7052. doi:10.5194/ACP-13-7039-2013
- Soja AJ, Al-Saadi JA, Giglio L, Randall D, Kittaka C, Pouliot GA, Kordzi JJ, Raffuse SM, Pace TG, Pierce T, Moore T, Roy B, Pierce B, Szykman JJ (2009) Assessing satellite-based fire data for use in the National Emissions Inventory. *Journal of Applied Remote Sensing* **3**, 031504. doi:10.1117/1.3148859
- Soja A, Fairlie T, Westberg D, Pouliot G (2012) Biomass burning plume injection height using CALIOP, MODIS and the NASA Langley Trajectory Model. 2012 US EPA International Emission Inventory Conference. Available at <https://www3.epa.gov/ttnchie1/conference/ei20/session7/asoja.pdf> [Verified 19 March 2021]
- Sokolik IN, Soja AJ, DeMott PJ, Winker D (2019) Progress and challenges in quantifying wildfire smoke emissions, their properties, transport, and atmospheric impacts. *Journal of Geophysical Research, D, Atmospheres* **124**, 13005–13025. doi:10.1029/2018JD029878
- Spinhirne JD (1993) Micro pulse lidar. *IEEE Transactions on Geoscience and Remote Sensing* **31**, 48–55. doi:10.1109/36.210443
- Spinhirne JD, Rall JAR, Scott VS (1995) Compact eye-safe lidar systems. *The Review of Laser Engineering* **23**, 112–118. doi:10.2184/LSJ.23.112
- Sullivan DC, Raffuse SM, Pryden DA, Craig KJ, Reid SB, Wheeler NJM, Chinkin LR, Larkin NK, Solomon R, Strand T (2008) Development and applications of systems for modeling emissions and smoke from fires: The BlueSky Smoke Modeling Framework and SMARTFIRE. Presented at the 17th International Emissions Inventory Conference led by the Environmental Protection Agency, Portland, OR, USA, 5 June 2008.
- Thomas JL, Polashenski CM, Soja AJ, Marelle L, Casey KA, Choi HD, Raut J-C, Wiedinmyer C, Emmons LK, Fast JD, Pelon J, Law KS, Flanner MG, Dibb JE (2017) Quantifying black carbon deposition over the Greenland ice sheet from forest fires in Canada. *Geophysical Research Letters* **44**, 7965–7974. doi:10.1002/2017GL073701
- Tosca M, Randerson J, Zender C, Nelson D, Diner D, Logan J (2011) Dynamics of fire plumes and smoke clouds associated with peat and deforestation fires in Indonesia. *Journal of Geophysical Research, D, Atmospheres* **116**, D08207. doi:10.1029/2010JD015148
- Tsaknakis G, Papayannis A, Kokkalis P, Amiridis V, Kambezidis HD, Mamouri RE, Georgoussis G, Avdikos G (2011) Inter-comparison of lidar and ceilometer retrievals for aerosol and Planetary Boundary Layer profiling over Athens, Greece. *Atmospheric Measurement Techniques* **4**, 1261–1273. doi:10.5194/AMT-4-1261-2011
- US Environmental Protection Agency (US EPA) (2018) 2014 National Emissions Inventory, Version 2 Technical Support Document. Available at [https://www.epa.gov/sites/production/files/2018-07/documents/nei2014\\_v2\\_tsd\\_05jul2018.pdf](https://www.epa.gov/sites/production/files/2018-07/documents/nei2014_v2_tsd_05jul2018.pdf) [Verified 19 March 2021]
- Val Martin M, Logan JA, Kahn RA, Leung FY, Nelson DL, Diner DJ (2010) Smoke injection heights from fires in North America: Analysis of 5 years of satellite observations. *Atmospheric Chemistry and Physics* **10**, 1491–1510. doi:10.5194/ACP-10-1491-2010
- Val Martin M, Kahn RA, Logan JA, Paugam R, Wooster M, Ichoku C (2012) Space-based observational constraints for 1-D fire smoke plume-rise models. *Journal of Geophysical Research, D, Atmospheres* **117**, D22204. doi:10.1029/2012JD018370
- Val Martin M, Kahn RA, Tosca MG (2018) A global analysis of wildfire smoke injection heights derived from space-based multi-angle imaging. *Remote Sensing* **10**, 1609. doi:10.3390/RS10101609
- van der Werf GR, Randerson JT, Giglio L, Collatz GJ, Mu M, Kasibhatla PS, Morton DC, DeFries RS, Jin Y, van Leeuwen TT (2010) Global fire emissions and the contribution of deforestation, savanna, forest, agricultural, and peat fires (1997–2009). *Atmospheric Chemistry and Physics* **10**, 11707–11735. doi:10.5194/ACP-10-11707-2010
- van Leeuwen TT, van der Werf GR, Hoffmann AA, Detmers RG, Rücker G, French NHF, Archibald S, Carvalho JA, Jr, Cook GD, de Groot WJ, Hély C, Kasischke ES, Kloster S, McCarty JL, Pettinari ML, Savadogo P, Alvarado EC, Boschetti L, Manuri S, Meyer CP, Siegert F, Trollope LA, Trollope WSW (2014) Biomass burning fuel consumption rates: a field measurement database. *Biogeosciences* **11**, 7305–7329. doi:10.5194/BG-11-7305-2014
- Walter C, Freitas SR, Kottmeier C, Kraut I, Rieger D, Vogel H, Vogel B (2016) The importance of plume rise on the concentrations and atmospheric impacts of biomass burning aerosol. *Atmospheric Chemistry and Physics* **16**, 9201–9219. doi:10.5194/ACP-16-9201-2016
- Welton EJ, Campbell JR (2002) Notes and correspondence: Micropulse lidar signals: uncertainty analysis. *Journal of Atmospheric and Oceanic Technology* **19**, 2089–2094. doi:10.1175/1520-0426(2002)019<2089:MLSUA>2.0.CO;2
- Westphal DL, Toon OB (1991) Simulations of microphysical, radiative, and dynamical processes in continental-scale forest smoke plume. *Journal of Geophysical Research* **96**, 22379–22400. doi:10.1029/91JD01956
- Whitehill AR, George I, Long R, Baker KR, Landis M (2019) Volatile organic compound emissions from prescribed burning in Tallgrass Prairie ecosystems. *Atmosphere* **10**, 464. doi:10.3390/ATMOS10080464
- Wilkins JL, Pouliot G, Foley K, Appel W, Pierce T (2018) The impact of US wildland fires on ozone and particulate matter: a comparison of measurements and CMAQ model predictions from 2008 to 2012. *International Journal of Wildland Fire* **27**, 684–698. doi:10.1071/WF18053
- Wilkins JL, de Foy B, Thompson AM, Peterson DA, Hyer EJ, Graves C, Fishman J, Morris GA (2020) Evaluation of stratospheric intrusions and biomass burning plumes on the vertical distribution of tropospheric ozone over the Midwestern US. *Journal of Geophysical Research: Atmospheres* **125**, e2020JD032454. doi:10.1002/essoar.10503951.1
- Winker D, Vaughan MA, Omar A, Hu Y, Powell KA, Liu Z, Hunt WH, Young SA (2009) Overview of the CALIPSO mission and CALIOP data processing algorithms. *Journal of Atmospheric and Oceanic Technology* **26**, 2310–2323. doi:10.1175/2009JTECHA1281.1
- Wooster MJ, Roberts G, Perry GLW, Kaufman YJ (2005) Retrieval of biomass combustion rates and totals from fire radiative power observations: FRP derivation and calibration relationships between biomass consumption and fire radiative energy release. *Journal of Geophysical Research, D, Atmospheres* **110**, D24311. doi:10.1029/2005JD006318
- Wotawa G, Trainer M (2000) The influence of Canadian Forest fires on pollutant concentrations in the United States. *Science* **288**, 324–328. doi:10.1126/SCIENCE.288.5464.324
- Zhou L, Baker KR, Napelenok SL, Pouliot G, Elleman R, O'Neill SM, Urbanski SP, Wong DC (2018) Modeling crop residue burning experiments to evaluate smoke emissions and plume transport. *The Science of the Total Environment* **627**, 523–533. doi:10.1016/J.SCITOTENV.2018.01.237

